

# Computational Studies of Ruthenium and Iridium Complexes for Energy Sciences and Progress on Greener Alternatives

Denis MAGERO

School of Science, Department of Chemistry and Biochemistry, Alupe University College, P.O. Box 845-50400, Busia, KENYA

e-mail: magerode@gmail.com

Tarek MESTIRI

Laboratoire de recherche (LR 18ES19), Synthèse asymétrique et Ingénierie moléculaire des Matériaux organiques pour l'Electronique organique, Faculté des Sciences de Monastir, Université de Monastir, 5000 Monastir, TUNISIA

e-mail: mestiri.tarek@gmail.com

Kamel ALIMI

Laboratoire de recherche (LR 18ES19), Synthèse asymétrique et Ingénierie moléculaire des Matériaux organiques pour l'Electronique organique, Faculté des Sciences de Monastir, Université de Monastir, 5000 Monastir, TUNISIA

e-mail: kamealimi@yahoo.fr

Mark Earl CASIDA

Laboratoire de Spectrométrie, Interactions et Chimie théorique (SITh), Département de Chimie Moléculaire (DCM, UMR CNRS/UGA 5250), Institut de Chimie Moléculaire de Grenoble (ICMG, FR2607), Université Grenoble Alpes (UGA) 301 rue de la Chimie, BP 53, F-38041 Grenoble Cedex 3, FRANCE

e-mail: mark.casida@univ-grenoble-alpes.fr

This manuscript has been prepared for submission as a book chapter for

Liliana MAMMINO (editor)

*Green Chemistry and Computational Chemistry,*

a volume in the *Advances in Green and Sustainable Chemistry Series,*

Due for publication July 2021,

Series list: <https://www.elsevier.com/catalog/all/all/all/advances-in-green-chemistry>

## Abstract

The energy sciences attempt to meet the increasing world-wide need for energy, as well as sustainability goals, by cleaner sources of energy, by new alternative sources of energy, and by more efficient uses of available energy. These goals are entirely consistent with the principles of green chemistry. This chapter concerns devices for creating electricity from light and for creating light from electricity. The major focus is on the photoproperties of ruthenium and iridium complexes, which have been proven to be a rich source of inspiration for conceiving photoactivated devices, including organic

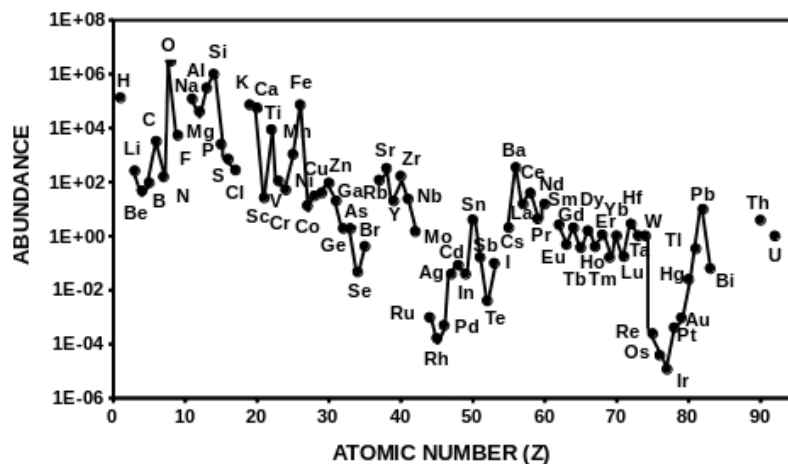


Figure 1: Relative abundance of different metals in the Earth’s continental crust in units of atoms of the element per  $10^6$  atoms of silicon. Figure adapted from Ref. [1].

photovoltaic (OPV) cells and organic light emitting diodes (OLEDs). The chapter reviews important already-in-use and potential applications of ruthenium and iridium complex-based photodevices, including the underlying mechanism behind their functioning and its investigation through computational chemistry approaches. It highlights the role of the information obtained from computational studies for the design of more efficient photodevices. The final part complements the discourse with a review of the progress on greener alternatives for OPVs and OLEDs.

## 1 Introduction

Alternative energy sources and alternative devices for making efficient use of energy fall nicely under the objectives of green chemistry. The most common source of energy nowadays remains the combustion of nonrenewable fossil fuels. Undesirable effects of fossil fuel combustion include air pollution contributing to global warming as well as political conflicts over the control of fossil fuel deposits. One of the objectives of green chemistry is to reduce the consumption of nonrenewable resources. Among the various alternatives to fossil fuels are photovoltaics (PVs). Solar energy is plentiful and solar cell (SC) technology promises to provide a ready source of relatively clean abundant energy for decades to come. Meanwhile light-emitting diode (LED) technology is revolutionizing how we light our homes and the displays on our computers, television, and phones. Although SCs and LEDs may seem unrelated, they are roughly speaking the same device run either “forward” to generate electrons from photons or run “backward” to generate photons from electrons. This makes the two particularly natural to discuss in a single chapter. This chapter focuses on particular types of SCs and LEDs, namely dye-sensitized solar cells (DSSCs) and organic LEDs (OLEDs). This choice is governed both by the authors’ expertise and by the importance of these devices on the broader field of PVs. At the heart of conventional DSSCs and conventional OLEDs is another green chemistry problem, namely the use of such rare elements (Fig. 1) as ruthenium (DSSCs) and iridium (OLEDs). After discussing conventional DSSCs and OLED technology and how computational chemistry helps to understand atomistic aspects of underlying processes and to create more efficient devices, still greener alternatives will be discussed that aim at eliminating rare metals from DSSCs and OLEDs.

The rest of this chapter focuses on the atomistic understanding of luminescent molecules as used

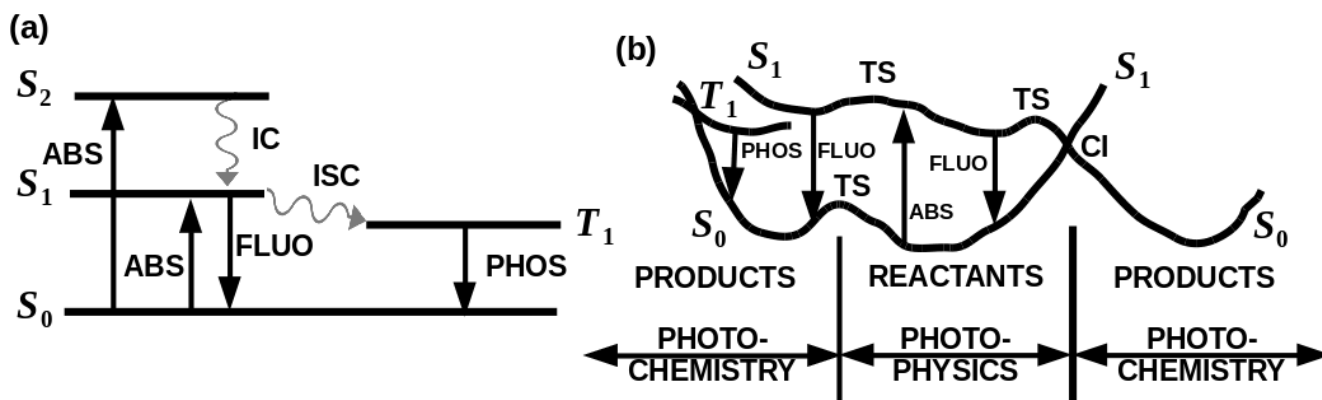


Figure 2: Two ways of representing photoprocesses: (a) Jablonski diagram, (b) potential energy curves (1D PESs.) Notation:  $S_0$ , ground singlet state;  $S_1$ , lowest excited singlet state;  $T_1$ , lowest triplet state; ABS, absorption; FLUO, fluorescence; PHOS, phosphorescence; ISC, intersystem crossing; CI, conical intersection; TS transition state.

in making photomolecular devices (PMDs [18]) such as DSSCs and OLEDs. Such devices often rely on the heavy-metal effect of ruthenium and iridium to enhance intersystem crossing probabilities. Some of current efforts to find greener solutions to replace rare metals will be reviewed. Emphasis will be placed on how computational chemistry is helping PVs. Section 5 concludes.

## 2 Photochemistry and Photodevices

This section provides a brief review of the science of photoprocesses followed by engineering aspects which are important for reading the scientific literature relevant to this chapter. The principles in this section are meant to be general. More system-specific principles will be discussed in subsequent sections.

### 2.1 Photochemistry

Photochemistry is usually defined as the study of light-induced chemical reactions. However chemiluminescence (the emission of light by chemical reactions) is also usually classed as photochemistry. Notice that there is an obvious analogy between solar cells (electricity generated by light) and photochemistry (in the sense of reactions generated by light) as well as an obvious analogy between light emitting diodes (light generated by electricity) and chemiluminescence, in part because of the electrochemical nature of SCs and LEDs. In fact, as we shall see, photovoltaics looks much like photochemistry (in the most general sense) when examined at the atomic scale. Here we only touch on some basic concepts and vocabulary from photochemistry. No attempt is made to review all of photochemistry; we are only setting the stage for later sections. For those seeking more in-depth treatments of photochemistry, we may direct them to any one of a number of excellent books [2, 3, 4, 5].

As Fig. 2 shows, photochemistry is a game played on several levels. Jablonski diagrams [such as Fig. 2(a)] represent these levels by simple lines and photochemical processes by straight arrows if light is absorbed or emitted and by wiggly lines if light is emitted. Modern photochemistry is based upon different potential energy surfaces (PESs), one for each electronic state (strictly speaking we will be

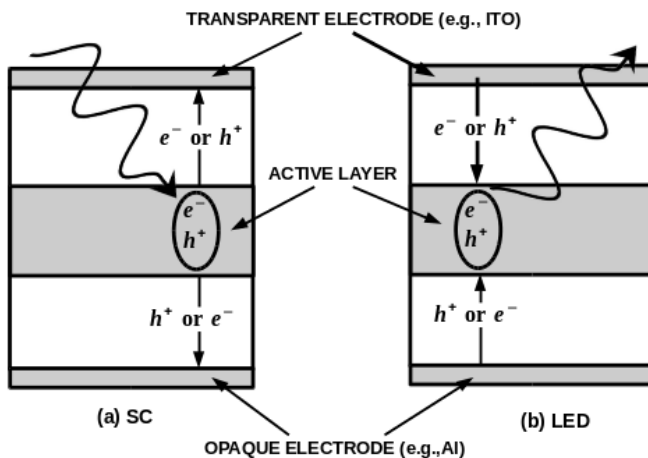


Figure 3: A schematic representation of how a solar cell (a) and how a light-emitting diode (b) work. The wiggly line represents light. See text for a more detailed description.

using the notion of adiabatic PESs though diabatic PESs are often also used.) If only one degree of freedom (e.g., some hypothetical reaction coordinate) is considered, then we have a 1D cross section (or potential energy curves) as shown in Fig. 2(b). Of the various processes shown in Fig. 2, the luminescent processes are the most important for this chapter. There are two of these, namely (i) fluorescence (FLUO) which is a spin-allowed photon emission between states of the same multiplicity from a short-lived excited state with a lifetime of  $10^{-12}$  to  $10^{-16}$  s and (ii) phosphorescence (PHOS) obtained after a change of spin [intersystem crossing (ISC)] due to spin-orbit coupling (SOC) to an excited state with longer lifetimes on the order of  $10^{-3}$  to  $10^{-2}$  s.

We will be concerned with the efficiency of different photoprocesses, such as luminescence. Let us consider a generic process  $x$ . The quantum yield  $\Phi_x$  of  $x$  is defined mathematically as,

$$\Phi_x = \frac{\text{number of molecules undergoing process } (x)}{\text{number of photons absorbed}} = \frac{\text{rate of process } (x)}{\text{rate of light absorption}}. \quad (1)$$

This is related to the rate constant  $k_x$  of this process and to the rate constants  $k_y$  of this ( $y = x$ ) and of competing ( $y \neq x$ ) processes,  $\Phi_x = k_x / (\sum_y k_y)$ . Rates may alternatively be described in terms of lifetimes  $\tau_x = 1/k_x$ . The lifetime of an excited state depends upon the rates of all the de-activation pathways,  $\tau = 1 / (\sum_y k_y)$ .

## 2.2 Solar Cells

Figure 3(a) shows a schematic representation of an organic SC. There are two electrodes, at least one of which must be transparent to let light enter the SC. A typical transparent conducting material for this purpose is indium tin oxide (ITO). These electrodes may be protected by additional layers to prevent corrosion and/or the formation of unwanted electronic effects. Sandwiched between the electrodes are a hole ( $h^+$ ) conducting donor (D) layer and an electron ( $e^-$ ) conducting acceptor (A) layer. These may be solid or stacked nanoparticles or even liquid, may be molecular or polymeric. Between the A and D layers is what we shall refer to as the active layer. This active layer may or may not be a different substance. For example, in a polymer heterojunction SC, the active layer is simply a region a few nanometers thick which is close enough to the heterojunction for the exciton

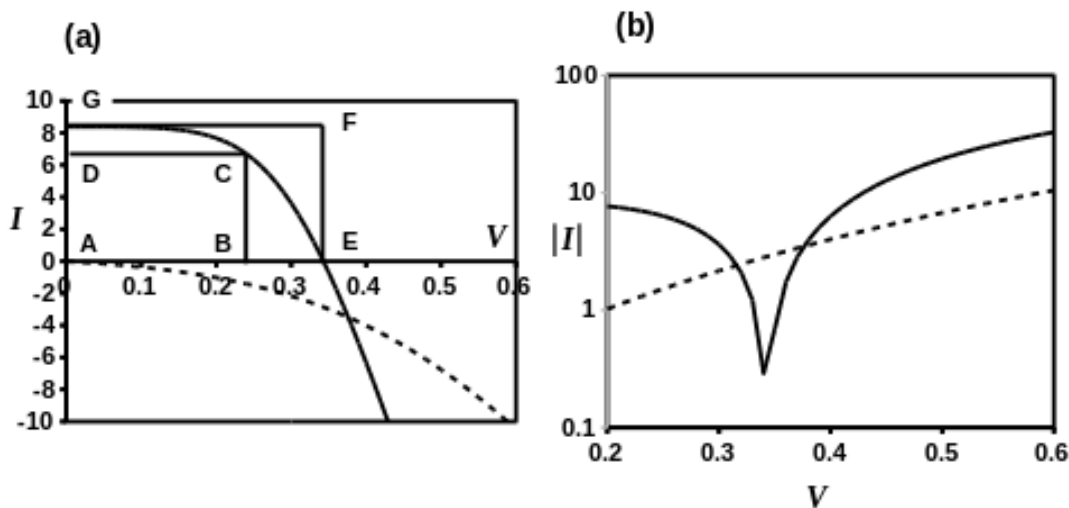


Figure 4:  $I$ - $V$  curves calculated with Eq. (4): solid curve (illuminated), dashed curve (without light.)  $V$  in volts;  $I$  in  $\mu\text{A}$ . The rectangles in part (a) are used to calculate the fill factor as described in the text. Part (b) is an alternate representation of the same data which is often used in the literature. Parameters used in the calculation:  $R = 0.01 \text{ M}\Omega$ ,  $V_T = 0.1 \text{ V}$ ,  $n = 1.5$ ,  $I_0 = 0.4 \mu\text{A}$ ,  $I_{ph} = 8 \mu\text{A}$ .

to arrive safely without undergoing  $e^-/h^+$  recombination. This heterojunction may be simple in form or even take on a highly convoluted shape composed of spaghetti-like interpenetrating D and A layers. In a Grätzel (or Graetzel, as German allows “ä” to be typed as “ae”) cell, the active layer consists of a dye adsorbed onto  $\text{TiO}_2$  nanoparticles which form the A layer. So, Fig. 3 is indeed very schematic as it is intended to cover a variety of cases.

The SC works by light creating an electron/hole ( $e^-/h^+$ ) pair (also known as an exciton) within the active layer. The electron then diffuses into the A layer and the hole into the D layer where they make their way to their respective electrodes and generate electricity. In the case of particular types of SCs, each step of this mechanism might be broken down into further steps, but this simple description of the mechanism is adequate for present purposes.

Experimentally, the performance of a SC is characterized in terms of the current,  $I$ , measured as a function of an applied voltage,  $V$ , under illumination. An  $I$ - $V$  curve is obtained similar to that shown in Fig. 4. The fill factor, FF, is defined as the ratio of the area of the rectangle (ABCD) of maximal area that can be placed under the  $I$ - $V$  curve to the area of the smallest rectangle (AEFG) containing the  $I$ - $V$  curve defined by the product of the short-circuit current,  $I_{sc}$  (at  $V = 0$ ), with the open-circuit voltage,  $V_{oc}$  (at  $I = 0$ ),

$$\text{FF} = \frac{I_m V_m}{I_{sc} V_{oc}}, \quad (2)$$

where  $I_m$  and  $V_m$  are the values at point C. To quote Grätzel [6], “The value of the fill factor reflects the extent of electrical (Ohmic) and electrochemical (overvoltage) losses.” If we also know the power density,  $P_s$ , of illumination, then we can calculate the SC photoconversion efficiency (PCE),  $\eta$ ,

$$\eta = \frac{I_{sc} V_{oc} \text{FF}}{P_s}. \quad (3)$$

This formula can be shown to be equivalent to the ratio of the electrical power generated by the SC to the light power absorbed. It is usually determined at AM 1.5G conditions, meaning using the solar spectrum at ground level as seen through an air mass of 1.5 times that of the atmosphere (to account for longer light paths when the sun is not directly overhead.) Schokley and Queisser showed that  $\eta$  has a thermodynamic upper limit of 44% [7]. The modern accepted theoretical upper limit is 34% at AM 1.5G. Note that this value is only for simple SCs, as opposed to, say, SCs created by stacks of simple SCs. Figure 4 was constructed using the Schokley diode equation with an added photocurrent term  $I_{ph}$ ,

$$I = I_0 \left( 1 - e^{\frac{V+IR}{nV_T}} \right) + I_{ph}. \quad (4)$$

Here  $V_T = kT/e$  is the thermal voltage, expressed in terms of Boltzman's constant  $k$ , the temperature  $T$  (in Kelvin), and the (absolute value of) the charge of the electron  $e$ . The diode ideality factor,  $1 \leq n \leq 2$ , is introduced to take electron relaxation into account. The Schokley diode equation is a standard way to describe conventional inorganic semiconductor devices [8] but it is also widely used to describe organic devices [9], although the underlying physics may be very different than for inorganic devices [10]. Of course, LEDs and OLEDs are governed by similar equations.

The easiest quantity to model in Eq. (3) is the open-circuit voltage,  $V_{oc}$ , at least under some idealized assumptions. In particular, Schokley and Queisser introduced the two detailed balance assumptions that: (i) every photon whose energy is greater than the fundamental gap  $E_g$  is absorbed, and (ii) every absorbed photon creates an electron-hole pair. It can then be shown that,

$$eV_{oc} \leq E_g = IP_D - EA_A, \quad (5)$$

where the fundamental gap  $E_g$  is the difference between the electron affinity of the acceptor,  $EA_A$ , and the ionization potential of the donor,  $IP_D$ . Empirically it has been found in certain cases that,

$$eV_{oc} = IP_D - EA_A - \text{constant} \approx (\epsilon_{\text{LUMO}}^A - \epsilon_{\text{HOMO}}^D) - \text{constant}, \quad (6)$$

where the constant reflects the nature of the electrode contacts and band bending effects in the particular SC [11]. The orbital energy approximation in Eq. (6) is valid to the extent that a Koopmans-like theorem holds [12]. Thus, within this approximation,  $V_{oc}$  may be optimized by designing the D and A components to have desirable relative HOMO and LUMO energies.

## 2.3 Light-Emitting Diodes

Figure 3(b) shows a very schematic representation of an LED. It should be clear that an LED is "just a SC run backwards," so that some of the same descriptive physics applies. For example, plots such as that in Fig. 4 are also common in the LED literature but typically also include the radiance of the LED on the same plot which is often roughly proportional to the current.

The external efficiency of an LED may be described phenomenologically by the equation,

$$\eta_{\text{ext}} = \chi_{\text{out}} \beta \gamma \Phi_{\text{PL}}, \quad (7)$$

where  $\chi_{\text{out}}$  is the optical coupling factor which describes light loss due to the interface with the transparent electrode,  $\beta$  describes the fraction of excitations that emit light,  $\gamma$  is the charge balance factor which describes the ratio of charge recombination to charge injection, and  $\Phi_{\text{PL}}$  is the photoluminescence (PL) quantum yield [17]. If the interest is in, say, interior lighting, then multiplication by the color rendering index (CRI) may also be appropriate, though it is not included in Eq. (7). The two factors of greatest importance for us are  $\beta$  and  $\Phi_{\text{PL}}$ , though we will also say a word about  $\gamma$

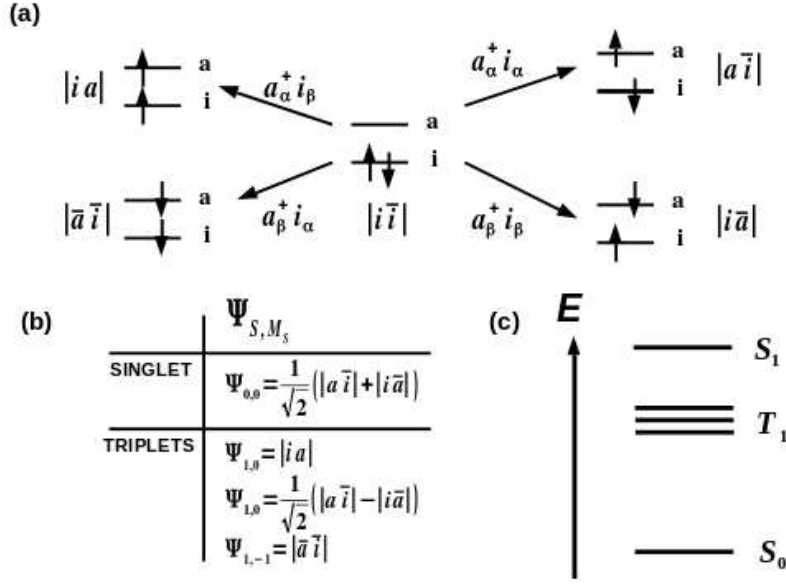


Figure 5: Two-hole two-electron model (TOTEM): (a) ground and singly excited states, (b) spin-adapted wave functions, and (c) Jablonski diagram. See text for additional explanation.

at the appropriate point below. The PL efficiency is related to radiative versus nonradiative factors. In particular, radiative rates ( $k^r$ ) should be maximized relative to nonradiative rates ( $k^{nr}$ ) so as to maximize,  $\Phi_{\text{PL}} = k^r / (k^r + k^{nr})$ .

Let us consider what happens when the electron and the hole meet in the active layer. To do this, we will consider the two-hole two-electron model (TOTEM) shown in Fig. 5. There are two orbitals. The lower-energy orbital  $\psi_i$  is doubly occupied and the higher-energy orbital  $\psi_a$  is empty in the ground state (GS). Simultaneous hole migration into  $\psi_i$  and electron migration into  $\psi_a$  leads to the four single determinant wavefunctions shown in part (a) of the figure. These are not all true excited states (ESs) as not all of them are spin eigenfunctions. Solving the Schrödinger equation in the absence of spin-orbit coupling leads to the spin-adapted wave functions shown in part (b) of the figure. Relative to the  $S_0$  GS, the corresponding open-shell singlet ( $S_1$ ) and triplet ( $T_1$ ) ES energies are,  $\Delta E_S = \epsilon_a - \epsilon_i + 2[ai|ia] - [aa|ii]$ , where  $\epsilon_i$  and  $\epsilon_a$  are orbital energies,  $[aa|ii]$  is a Coulomb repulsion integral, and  $[ai|ia]$  is an exchange integral. We have the classic result that the corresponding open-shell singlet ES is higher in energy than the triplet. This leads to the Jablonski diagram shown in part (c) of the figure. As photons carry no spin, radiation selection rules predict that fluorescence ( $S_1 \rightarrow S_0$ ) is allowed, while phosphorescence ( $T_1 \rightarrow S_0$ ) is forbidden. We can now understand the most fundamental problem in LED theory which is that the fraction of excitations that emit light nominally is only  $\beta = 1/4$  in Eq. (7) in the absence of spin-orbit coupling. We shall call this the spin-statistics problem. It also leads to a lowering of the PL efficiency. Altogether the result is an unacceptable inefficiency in LEDs. Later, in Secs. 3.3 and 4.3, we will discuss various strategies used to overcome the spin-statistics problem.

### 3 Heavy Metal Complex Photoprocesses

At the heart of every photodevice are atomistic-level photoprocesses. For the cases discussed in this section and in the next section (Sec. 4), namely dye-sensitized solar cells (DSSCs) and organic LEDs

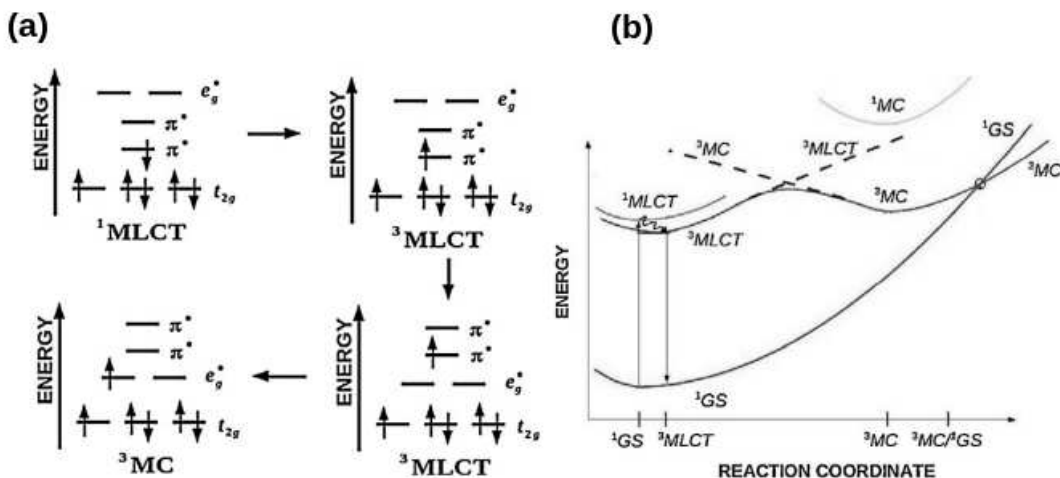


Figure 6: (a) Ligand field theory diagrams for the electronic ground state and the most relevant excited state of a pseudo-octahedral  $d^6$  complex. Adapted from Ref. [21]. (b) The principle PES expected from LFT. The dashed lines indicate diabatic states whose avoided crossing leads to the energetic barrier on the adiabatic surface between the  $^3\text{MLCT}$  and  $^3\text{MC}$  minima. Adapted from Ref. [21].

(OLEDs), there are specific molecules that capture light to produce electrons or capture electrons to produce light. The former are examples of photochemical molecular devices (PMDs) which have been defined as structurally organized and functionally integrated systems capable of elaborating the energy and information input of photons to perform complex functions [18]. PMDs, DSSC dyes, and sensitizers for OLEDs may all be viewed as particular cases of molecular electronics, whose origin is usually attributed to Aviram and Ratner in their famous 1974 article [19]. Because of lack of practical applications, molecular-level electronics is sometimes viewed as only an emerging field, and yet we are about to delve into some very practical present-day examples of molecular electronics!

### 3.1 Traditional Model

The most frequently used dye in DSSCs is some form of (pseudo-)octahedrally-coordinated polypyridinal ruthenium(II) complex and a (pseudo-)octahedrally-coordinated polypyridinal iridium(III) complex is commonly introduced into the active layer of organic LEDs (OLEDs). The traditional model for describing the electronic structure of the ground and excited states of such complexes is, of course, ligand field theory (LFT) [20]. Even though *ab initio* and density-functional methods have evolved to the point that they may now be applied to these complexes, LFT cannot be avoided because it remains the language used in discussing these complexes. In fact, one problem is how to recover an LFT picture from DFT so that computational chemists using DFT can speak with experiments in a familiar LFT language.

The  $O_h$  LFT splitting of the 5  $d$  orbitals into three lower  $t_{2g}$  and two higher  $e_g$  orbitals is familiar from most university first-year chemistry courses. As we will typically be dealing with high-field splitting, the expected GS LFT configuration is  $t_{2g}^2 e_g^4$ . The  $t_{2g}$  orbital is nonbonding with polypyridinal ligands, but the  $e_g$  orbital is actually antibonding. Different from in the first-year courses, we will emphasize this by writing  $e_g^*$ . Polypyridinal ligand  $\pi^*$  orbitals are energetically interspersed between the  $t_{2g}$  and  $e_g^*$  orbitals.

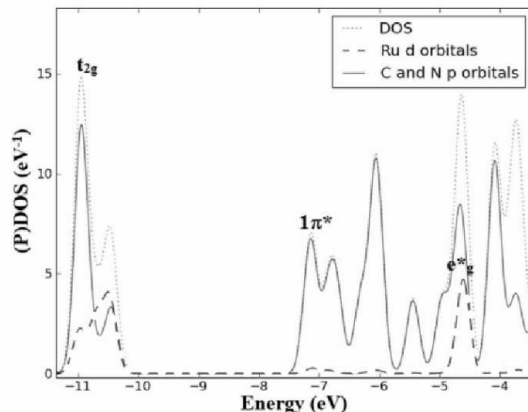


Figure 7: PDOS for a polypyridinal ruthenium(II) complex. Adapted from Ref. [21].

We are now in a good position to be able to understand the ESs and associated photoprocesses of our complexes [Fig. 6(a)] [18, 22, 23]. They are, of course, governed by the same general principles already described in Sec. 2.1. When a photon is absorbed by the singlet GS ( $^1\text{GS}$ ), the spin-selection rule tells us that the initial excited-state will also be a singlet. Furthermore the Laporte selection rule forbids  $d \rightarrow d$  metal centered (MC) transitions, so we should expect the initial excited state to be of metal-ligand charge-transfer (MLCT) character. This may not be the same  $^1\text{MLCT}$  ES shown in the upper right-hand side (RHS) of Fig. 6(a), but radiationless relaxation will soon bring us down to this latter  $^1\text{MLCT}(t_{2g}, \pi^*)$  state. No great change in geometry is expected at this point. However SOC due to the heavy-metal effect [24, 25] means that ISC can occur to populate the corresponding triplet state  $^3\text{MLCT}(t_{2g}, \pi^*)$  [lower RHS of Fig. 6(a)]. If this is close enough to the  $^3\text{MC}(t_{2g}, e_g^*)$  state, then configuration mixing will occur, allowing a transformation of the  $^3\text{MLCT}$  character of the ES to  $^3\text{MC}$  character [lower left-hand side (LHS) of Fig. 6(a)]. As the  $\pi^*$  orbital is antibonding only within the ligand but the  $e_g^*$  orbital is antibonding between the ligand to the metal, the  $^3\text{MLCT}$  state is expected to have approximately the same geometry as the  $^1\text{GS}$  but the  $^3\text{MC}$  state is expected to have a longer metal ligand bond length in comparison with the  $^1\text{GS}$ . All of this is illustrated in Fig. 6(b) where we also see the possibility of a triplet transition state ( $^3\text{TS}$ ) between the  $^3\text{MLCT}$  and the  $^3\text{MC}$  state. Also shown in Fig. 6(b) is the crossing of the  $^1\text{GS}$  and  $^3\text{MC}$  curves at large metal-ligand bond distance. At this point, partial dissociation of the complex and/or interaction with the solvent, combined with the heavy-metal effect, allows radiationless relaxation of the  $^3\text{MC}$  state back to the  $^1\text{GS}$ . Not shown in Fig. 6(b) is the expected Jahn-Teller distortion of the MLCT and MC states due to the electronic degeneracy (or near degeneracy) of the orbital configuration. This LFT picture tells us that our complexes will have long-lived (phosphorescent) excited states because of the spin-forbidden nature of the  $^3\text{MLCT} \rightarrow ^1\text{GS}$  transition. We still have the problem of recovering a LFT picture from more sophisticated calculations. Quantitatively correct geometries may be obtained from DFT and TD-DFT is commonly used to calculate absorption spectra, but a connection to LFT is still needed. This is not really a problem for the nonbonding  $t_{2g}$  orbitals which can often be readily identified by visualizing the molecular orbitals of the complex but the same method rarely allows identification of the antibonding  $e_g^*$  orbitals because they are heavily mixed with ligand orbitals. Nevertheless we have found that a LFT-like picture may be recovered from DFT calculations using the partial density of states (PDOS) method [26]. Figure 7 shows (dotted

line) the total density of states,

$$\text{DOS}(\epsilon) = \sum_i g(\epsilon - \epsilon_i), \quad (8)$$

of a polypyridinal ruthenium (II) complex. Here the  $\epsilon_i$  are the energies of the occupied and unoccupied orbitals and  $g$  is a normalized gaussian broadening function ( $\int g(x) dx = 1$ ). The partial DOS (PDOS) uses Mulliken population analysis to assign how much of the DOS is due to metal  $d$  orbitals and how much is due to ligand  $\pi$  and  $\pi^*$  orbitals. (The concepts of DOS and PDOS are extensively discussed in the context of surface chemistry in Ref. [27].) Specific formula for the PDOS are given in the supplementary material associated with Ref. [26]. Suffice it to say that the gaussian broadening combined with the Mulliken population analysis allows us a clear picture (shown in Fig. 7) of where the  $t_{2g}$  and  $e_g^*$  orbitals lie, even though some inevitable fuzziness remains due to the necessary choice of the full width at half maximum (FWHM) of the gaussian broadening and some basis-set-dependence in the Mulliken population analysis. It should also be noted that the  $e_g^*-t_{2g}$  energy difference calculated in this LFT-like approach is not the same as that in true LFT but still provides a useful LFT-like picture. We will return to the use of the PDOS in Sec. 3.4 when we discuss an orbital-based luminescence index.

### 3.2 Ruthenium Complexes in Dye-Sensitized Solar Cells

The first DSSC was that of O'Regan and Grätzel in 1991 [28]. In 2017, Michael Grätzel received the Global Energy Prize “for transcendent merits in development of low cost and efficient solar cells, known as ‘Graetzel cells’ ” [29] or DSSCs. DSSCs are composed of a sensitizing dye that is adsorbed at the surface of nanoparticles made of a wide band-gap semiconductor [titanium oxide ( $\text{TiO}_2$ ) in the original DSSC]. The dye absorbs light and transfers an electron to the semiconductor conduction band. The hole left in the dye is regenerated by a solution redox electrolyte [a triiodide/iodide ( $\text{I}_3^-/\text{I}^-$ ) redox couple in the original DSSC] or a solid hole conductor and finally the electron migrates through the external load to complete the circuit [30, 6, 31, 32]. The nanoparticulate nature of the semiconductor is critical as it provides a large surface area for grafting a large amount of dye [28, 33, 34, 35, 36, 37, 38, 39]. Charge separation occurs (in  $n$ -type DSSCs) through photo-induced electron injection from the dye into the conduction band of the solid nanoparticles [30, 6, 31, 32]. Evidently the  $S_1$  excited state of the dye must be higher in energy than the oxide conduction band (CD) and the electrolyte redox couple must also be able to replenish the dye with a new electron [40, 41].

The original 1991 DSSC had a 7.9% efficiency under a light intensity of  $8.3 \text{ mW.cm}^{-2}$  (AM 1.5G) and of 7.12% under a light intensity of  $75 \text{ mW.cm}^{-2}$  (AM 1.5G). Much work has been done to improve this efficiency by working on the different DSSC components [42, 43, 44, 45, 46]. The dye in the DSSC assembly plays a particularly significant role in the harvesting of solar energy and its conversion into electrical energy. Consequently much work has been done on improving the dye by various strategies ranging from incorporating functionalized ancillary ligands such as triazolylpyridine to replacing the thiocyanate ligands with other chelating anions [47]. The result has been consistent improvement in efficiency to more than 11% using *tris*(2,2-bipyridyl)ruthenium(II) analogues [48]. One of the very best dyes has turned out to be  $[\text{Ru}(\text{tcterpy})(\text{NCS})_3]$  (tcterpy=4,4',4''-tricarboxy-2,2':6',2''-terpyridinne), also known as “N749” or as the “black dye” because of its ability to absorb a remarkably large part of the solar spectrum [49, 50, 51, 52].

At the present time, DSSCs have been commercialized and are being sold by a number of companies, including Dysol, Solaronix, SolarPrint, G24innovations, Sony Corporation, H.Glass, and Exeger Operations AB. The energyglass facade of the Science Tower in Austria is the largest installation

so far of DSSCs and was manufactured by H.Glass.

### 3.3 Iridium Complexes in Organic Light Emitting Diodes

The basic theory of LEDs was already presented in Sec. 2.3. Thanks to work recognized by the 2000 Nobel Prize in Chemistry which was awarded to Alan J. Heeger, Alan G. MacDiarmid, and Hideki Shirakawa “for the discovery and development of conductive polymers” organic LEDs (OLEDs) are now possible. These provide efficient light sources for lighting and displays. Expertise in organic chemistry means that OLEDs are arguably easier to fine tune and can be made more cost efficiently. In particular, this helps in engineering color-tunability, colour quality, luminance efficiency, large-area display, wide-viewing angle, and lightness. Also, OLEDs have the advantage over conventional LEDs in that they can be made flexible [53]. For all of these reasons, OLEDs are now a well-established commercial success story. This section describes conventional OLEDs, based upon the “heavy atom effect.” (Reviews may be found in Refs. [55, 56, 17].)

These OLEDs make use of the so-called “heavy atom effect”—that is, the presence of significant spin-orbit coupling (SOC) due to the presence of heavy atoms. This leads not only to lifting of the degeneracy between the triplet states but also to singlet-triplet mixing and allows rapid conversion of the singlet into a triplet through ISC. At the same time, a singlet component is introduced into the triplet states so that they may radiate by phosphorescence. The resultant OLED is thus a phosphorescent OLED. Care must be taken in ligand design to minimize nonradiative decay. One way to do this is by assuring short phosphorescence lifetimes. This is also important in designing OLEDs with values of  $\gamma$  [Eq. (7)] close to unity when operating at high power so that energy is dissipated quickly before other processes can take place. The rest of this section is devoted to describing the particular role of the different electronic states involved when metal complexes are used in OLEDs. The reader interested in further information about this classic type of OLED is referred to Refs. [55, 56, 17].

As the SOC constant ( $\zeta$ ) increases as the fourth power of the effective nuclear charge  $Z$ , then the most effective elements for introducing SOC are the heavy elements. Of these, the heavy metal ion iridium(III) is generally considered the most important OLED emitter [55]. Indeed, the conventional solution to the spin-statistics problem dates back to 1999 when iridium phenylpyridine complexes were introduced into the active layer [54]. These OLEDs make use of the so-called “heavy atom effect.” The high  $\zeta$  values for iridium(III) and the large choice of ligands whose energy levels mix well with atomic orbitals of iridium(III) has necessitated the development of materials that emit with very high efficiency from triplet states. Not only do iridium(III) complexes emit from states with a large degree of MLCT character [57], but iridium(III) complexes are also highly emissive at room temperature, possess radiative lifetimes in the range of microseconds, which are advantageously shorter than the typical lifetimes of pure organic phosphorescent materials [58]. This in turn improves the quantum efficiency of OLEDs to values as high as 100%.

Iridium complexes have already been used successfully in the design of efficient phosphorescent emitters in OLEDs [59, 60, 61, 62, 57, 63, 64, 17, 65, 66, 67, 68, 69, 70]. In particular, cyclometallated iridium(III) complexes have and are still in use as an OLED phosphors. The archetypal structural unit of an iridium(III) complex comprises an aryl heterocycle, often a 2-phenylpyridine unit, that is bound to the metal through the heteroatom of the heterocycle and through a metallated carbon atom *ortho* to the interannular bond [71]. An example is *fac*-Ir(ppy)<sub>3</sub> shown in Fig. 8(a).

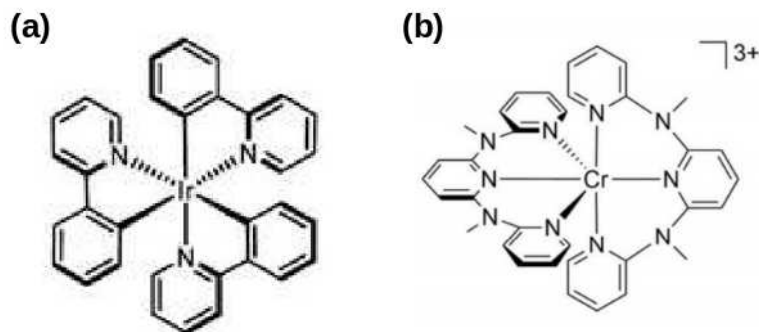


Figure 8: (a) *Fac*-tris-phenylpyridineiridium(III), *fac*-Ir(ppy)<sub>3</sub>, ppy = 2-phenylpyridine. (b) “Molecular ruby”:[Cr(ddpd)<sub>2</sub>]<sup>3+</sup> [80, 84, 85, 86].

### 3.4 Modeling Luminescence

Luminescence plays a key role in the theory of both DSSCs and OLEDs. In the DSSC case, the longer the luminescence lifetime, the greater the chance of transferring an electron to the nanoparticulate semiconductor. In the OLED case, we wish to obtain as much light as possible through phosphorescence. The traditional model for luminescence in octahedrally-coordinated polypyridinal ruthenium(II) and iridium(II) complexes has been explained in Sec. 3.1. It is used both as an explanation of luminescence and as a hypothetical model for designing complexes with long-lived luminescent states even though the basic model was initially developed for [Ru(bpy)<sub>3</sub>]<sup>2+</sup>. Our goal in this section is to go beyond [Ru(bpy)<sub>3</sub>]<sup>2+</sup> and to validate this model, if possible, for the entire class of octahedrally-coordinated polypyridinal ruthenium(II) complexes. As will soon become clear, this is an ambitious goal which requires us to make some drastic compromises. Nevertheless the result will be an orbital-based luminescence index (LI) which seems to work remarkably well [21].

Experimental luminescence lifetimes measure the rate of disappearance of the excited state *either* by luminescence *or* by other mechanisms such as radiationless relaxation. Hence competing radiationless relaxation routes can lead to significant reductions in luminescence lifetimes. According to the traditional model (Sec. 3.1), we are particularly interested in <sup>3</sup>MLCT → <sup>3</sup>MC pathway shown in Fig. 6(b) and whose rate is determined by the height of the <sup>3</sup>TS barrier. Unfortunately finding the value of the height of this barrier is not easy to do experimentally. It involves measuring luminescence lifetimes at many temperatures and then fitting them to an elaborate empirical form [72]. Moreover sufficiently complete temperature information for empirical fitting is only available for a few compounds, one of which is tris(bipyridine)ruthenium(II) [Ru(bpy)<sub>3</sub>]<sup>2+</sup> in propionitrile/butylnitrile (4:5 v/v) where the height of the <sup>3</sup>TS barrier is 3 960 cm<sup>-1</sup> [72].

Another way to determine the height of the <sup>3</sup>TS is theoretically using DFT. This is not as straightforward as it may at first sound. In general, the triplet surface exhibits multiple different <sup>3</sup>TSs. This is especially true in the case of a complex with several different types of ligands, but is also true in the case of a complex with a single type of ligand. In the later case, there are not only barriers for removing ligands but also barriers for pseudorotations between different Jahn-Teller distorted geometries. To find the right <sup>3</sup>TS, it is first necessary to have a guess as to how the reaction might proceed. Here we may be guided by Adamson’s rules which say that (1) the weakest bond will break if one bond is weaker than the others or else (2) two bonds will break *trans* to each other in the case that all bonds are of similar strength [73]. What is typically done once a pathway is decided upon is to vary some representative coordinate while relaxing all other coordinates (“do a

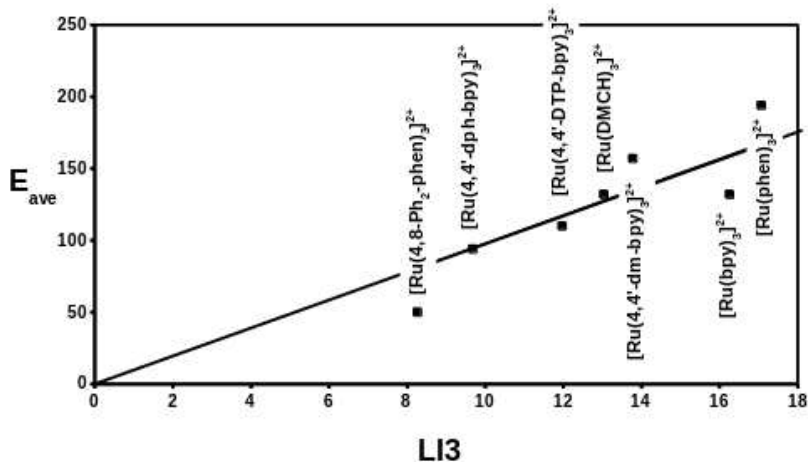


Figure 9: Performance of luminescence index number 3 for complexes of formula  $[RuX_3]^{2+}$ . Both LI3 and  $E_{ave}$  are in  $cm^{-1}$ . Adapted from Ref. [21]. See this same reference for a definition of the ligand names.

scan”) to find a possible TS. Convergence to this TS may be tightened using special methods and vibrational frequencies are calculated to insure that it is indeed a real TS with a single internal vibrational frequency. In the past, some authors made the error of identifying the scan path with the reaction path. However this is quite incorrect [74]. Instead the intrinsic reaction coordinate (IRC) is calculated by following the PES down in energy on each side towards the reactants and the products. Only then can the true activation energy of the reaction be determined. Besides the much studied  $[Ru(bpy)_2]^{2+}$  complex [75, 76, 77], Sun *et al.* have determined the  $^3TS$  and activation energy for two ruthenium(II) compounds ( $[Ru(mpy)_2]^{2+}$  and  $[Ru(mphen)_2]^{2+}$ ) [76]. The results require careful examination as they are subject to variations upon choice of functional and variations in the quality of the basis sets. The gas phase theoretical values of the  $^3TS$  activation energy for *cis* dissociation ( $1\,364\,cm^{-1}$  [75] and  $1\,136\,cm^{-1}$  [76]) and for *trans* dissociation ( $700\,cm^{-1}$  [77]) of  $[Ru(bpy)_3]^{2+}$  may be compared with the above mentioned experimental value of  $3\,960\,cm^{-1}$  in solution. It should also be kept in mind that “chemical accuracy” is at best  $1\,kcal/mol = 350\,cm^{-1}$  and that “transition metal accuracy” [78] is more like  $5\,kcal/mol = 1\,700\,cm^{-1}$ .

As trends are more important than absolute numbers, we decided to take another approach to extracting a  $^3TS$  energy from experiment. The review article of Juris *et al.* [72] provides almost 100 pages of data on photoprocesses for ruthenium(II) complexes with polypyridyl ligands. In many cases there is data at both liquid nitrogen (77 K) and room temperature (298 K). This is enough to obtain an “average activation energy”  $E_{ave}$  using the equation,

$$k(T) = A_{ave}e^{-E_{ave}/RT}. \quad (9)$$

We expect that this will underestimate the true  $^3TS$  activation energy ( $E_{ave} = 132\,cm^{-1}$  for  $[Ru(bpy)_3]^{2+}$ ) but we do expect it to preserve general trends. Moreover it is easier to analyze one parameter than have to deal with all six parameters that appear in the empirical formula of Ref. [72]. In the end of our analysis of the experimental results in Ref. [72], we have results for about a hundred complexes.

These results could be compared against calculated  $^3TS$  activation energies. However calculating  $^3TS$  activation energies for a hundred complexes is a formidable task. It also may be difficult to explain the results back in terms of a LFT-like model. We therefore opted for a less ambitious

Compound	$\lambda_{\text{abs}}$	$\lambda_{\text{em}}$	$\tau$
ruby <sup>a</sup>	407 nm	694 nm	4.268 ms
[Cr(ddpd) <sub>2</sub> ] <sup>3+,b</sup>	435 nm	778 nm	898 ns
[Ru(bpy) <sub>3</sub> ] <sup>2+,c</sup>	452 nm	615 nm	950 ns
[Ir(ppy) <sub>3</sub> ] <sup>d</sup>	375 nm	514 nm	1.9 $\mu\text{s}$

<sup>a</sup>Al<sub>2</sub>O<sub>3</sub>(s) doped with Cr<sup>3+</sup> [79], <sup>b</sup>In water [80], <sup>c</sup>Refs. [81, 82], <sup>d</sup>Refs. [83, 82].

Table 1: Examples of luminescent compounds.

approach, namely to build a LI based upon LFT-like orbital energies extracted from calculated PDOSs. Different LIs were proposed in Refs. [26, 21]. The one (LI3) that was found to work best [21] was not the most obvious choice but rather is based upon qualitative frontier-orbital-like reasoning,

$$\text{LI3} = \frac{\bar{E}^2}{\Delta E}, \quad (10)$$

where  $\Delta E = \epsilon_{e_g^*} - \epsilon_{\pi^*}$  and  $\bar{E} = (\epsilon_{e_g^*} + \epsilon_{\pi^*})/2$ . Figure 9 shows that LI3 is an excellent predictor of  $E_{\text{ave}}$  for polypyridine ruthenium(II) ligands composed of three identical bidentate ligands. The picture is not so clean when we include other polypyridine ligands [21], although we are quite happy with the performance of such a simple model, especially given the large number of approximations needed to extract  $E_{\text{ave}}$ . In particular, complexes with tridentate ligands appear to lie on a different line than complexes with bidentate ligands.

## 4 Greener Alternatives

This section discusses greener alternatives to ruthenium in DSSCs and to iridium in OLEDs. Luminescence useful for other photodevices is also considered. We first consider replacing of rare expensive metals with more less expensive abundant metals and then go on to considering how to eliminate metals entirely.

### 4.1 Earth-Abundant Transition-Metal Complexes

Luminescence is by no means restricted to complexes of rare expensive metals, but it is only within the last decade or less that attention has turned to making more efficient photodevices from less expensive Earth-abundant metals, including chromium, iron, copper, zinc, zirconium, molybdenum, and uranium [87]. Although most of the work has been done on copper(I) complexes, for reasons of space, we have chosen to focus on the story of how a “molecular ruby” was made by “rational ligand design” [80] through a close collaboration between researchers from coordination chemistry, physical inorganic chemistry, and spectroscopy [84].

Ruby is a form of aluminum oxide (Al<sub>2</sub>O<sub>3</sub>) called corundum with additional chromium impurities (Ref. [88], pp. 159-161, see also Ref. [89].) Cr<sup>3+</sup> ion replace Al<sup>3+</sup> ions in octahedral sites and are responsible for the well-known red color of ruby. There are three particularly important states which we will describe using LFT [20]. In order of decreasing energy, these are,

$${}^4T_2 : \underbrace{[\uparrow][\uparrow][\ ]]}_{t_{2g}} \underbrace{[\uparrow][\ ]]}_{e_g}, \quad {}^2E : \underbrace{[\uparrow][\downarrow][\uparrow]}_{t_{2g}} \underbrace{[\ ][\ ]]}_{e_g}, \quad {}^4A_2 : \underbrace{[\uparrow][\uparrow][\uparrow]}_{t_{2g}} \underbrace{[\ ][\ ]]}_{e_g}, \quad (11)$$

where the electron configuration from which each state is derived by symmetry projection is shown. Ruby luminesces at 694 nm with a long luminescence lifetime of 1.8  $\mu\text{s}$  [79] (Table 1.) This may be regarded as phosphorescence because the initial spin-conserving photoexcitation  ${}^4A_2 \rightarrow {}^4T_2$  leads to a radiationless intersystem crossing  ${}^4T_2 \rightarrow {}^2E$  with spin flip. The final luminescence comes from the  ${}^2E \rightarrow {}^4A_2$  transition which is nominally spin forbidden, leading to a long luminescence lifetime. This luminescence was exploited in making the first laser [90] (see also Ref. [91], pp. 104-106.)

Now suppose we want to make an octahedral Cr(III) coordination complex with properties analogous to, but ideally even better than, ruby by varying the ligands around the central metal atom. How should we proceed? It turns out that the main problem is the photoluminescence yield  $\Phi$  [Eq. (1)], namely the number of photons that luminesce in comparison to the number of photons that absorb.  $\Phi$  is low in Cr(III) complexes with low ligand field strength because the energy ordering of the states is, *Energy*:  ${}^2E > {}^4T_2 > {}^4A_1$ . As the  ${}^4T_2$  state is close in energy to the  ${}^4A_1$  state, the “energy gap law” which states that radiationless decay becomes more likely the closer an excited state is in energy to the ground state tells us to expect that  $\Phi$  will be very small. For conventional strong-field ligands, *Energy*:  ${}^2E \approx {}^4T_2 > {}^4A_1$ , which is also not good because the radiative  ${}^2E$  and the nonradiative  ${}^4T_2$  states readily exchange energy, hence lowering  $\Phi$ . Instead, we should seek a very strong-field ligand so that, *Energy*:  ${}^4T_2 > {}^2E > {}^4A_1$ , if we want to maximize  $\Phi$ .

The ligand that was found to satisfy these criteria gave a “molecular ruby” *bis*(N,N'-dimethyl-N,N'-dipyridine-2-ylpyridine-2,6-diamine)chromium(II) cation,  $[\text{Cr}(\text{ddpd})_2]^{3+}$  [Fig. 8(b)]. (Ref. [92] provides a comprehensive review of the ddpd ligand and its zinc, copper, nickel, cobalt, iron, chromium, and vanadium complexes.) Molecular ruby turns out to be very stable, water soluble, and to have a luminescence lifetime of 899  $\mu\text{s}$  with a photoluminescence yield of 11% [80] (Table 1.) It may be used to produce singlet oxygen [84], create an optical molecular thermometer [85], and as an alternative to ruby in measuring pressure in high pressure experiments [86]. Further improvement of the photoproperties of molecular ruby may be obtained by deuteration, giving a luminescence lifetime of 2.3 ms and a luminescence yield of 30% [93].

Let us now take a closer look at how computational chemistry helped in the design of molecular ruby. We should not forget that the starting point was LFT, which may be regarded as one of the tools in the computational chemists' toolbox. In fact, explicit LFT calculations were reported in Ref. [86] as well as DFT and complete active space self-consistent field (CASSCF) calculations. LFT tells us that we may increase the LFT splitting by choosing a strong-field ligand with a large bite angle, guaranteeing a rigid octahedral geometry, and by making sure that it is a strong  $\sigma$  donor. Note that a rigid geometry will also help to reduce vibrations which are associated with radiationless relaxation. The ddpd ligand was designed computationally with the aim in mind of synthesizing another complex, related to, but different from, molecular ruby [94]. Not every complex designed by computational chemists may be synthesized. In fact, the initially imagined complex could not be synthesized in this case [94]. However that investigation also included a computational investigation of  $[\text{Ru}(\text{ddpd})_2]^{2+}$ , showing that the *mer* isomer should be more stable than the *fac* isomer and that the bite angle of ddpd should be close to 90°. (In fact, the bite angle reported in Ref. [94] is 88°.) The bite angle in molecular ruby is in the range off roughly 85° - 87° (Table 1 of Ref. [92].) Once the compound was synthesized, it was necessary to characterize the product to prove that it is the correct compound. In this case, X-ray crystallography could prove that the compound was the correct one and photophysical methods could verify the spectra and photoluminescence yield, but computational chemistry is needed in order to validate the theoretical reasoning accounting for the photophysical properties. In Ref. [80], the theoretical reasoning was validated by using TD-DFT to assign the excited states, the calculation of excited state spin densities to validate that the chromium remains in the +III oxidation state, and the geometries of some of the excited states were optimized in order

to understand excited-state relaxation effects. Ref. [84] includes a report on the results of a DFT study of the reaction of  $^1\text{O}_2$  with a model amine  $\text{N}(\text{CH}_2\text{CH}_3)(\text{CH}_3)_2$ .

## 4.2 Organic Dye-Sensitized Solar Cells

As we have seen, one of the best dyes for use in DSSCs is triscarboxy-ruthenium terpyridine [ $\text{Ru}(4,4',4''\text{-(COOH)}_3\text{-terpy})(\text{NCS})_3$ ], popularly known as the “black dye.” However ruthenium is expensive (about 250 USD/ozt) and mildly toxic [95]. This has led to the desire to replace the black dye (and other heavy-metal containing dyes) by metal-free DSSC dyes. We give a brief review of metal-free DSSC dyes in this section. Some of these dyes are simply extracted from natural sources. Others are “engineered.” We follow up this literature review by an example from our own work of how computational chemistry can help in DSSC dye design.

Natural dyes containing carboxylic acid groups can easily react with the surface of  $\text{TiO}_2$  nanoparticles. Such dyes can often be extracted from plants, using green chemistry, without tedious synthesis, using relatively simple separation and purification methods. The resultant dyes may sometimes be used as metal-free dyes in functioning DSSCs. For example, in 1997, Grätzel and co-workers were among the first to report the use of natural dyes in a DSSC by using blackberry juice to create a working DSSC [97]. It is now even possible to find [youtube](#) videos explaining how to make your own DSSC using blackberry juice [98]. In recent years, the list of natural metal-free dyes for making DSSCs has considerably expanded. (References [99, 100, 101, 102] review the state of the natural dyes for use in DSSCs.) Unfortunately, typical PCEs are very low (less than 1%). Hence, molecular-level engineering to create better MF DSSC dyes seems quite warranted. In this context, computational chemistry modeling can hope to provide a molecular-level understanding which can help in optimizing photoefficiency. Indeed, there are many beautiful computational chemistry studies in the literature, including (but not limited to) Refs. [104, 105, 106, 107, 108, 109, 110, 111, 112, 113]. Let us just mention an explicit solvent molecular dynamics/TD-DFT study of the color of alizarin bound to  $\text{TiO}_2$  as a particularly detailed study of a particular system [107]. However, rather than study a specific system in detail, most studies seek to understand trends for series of candidate metal-free DSSC dyes.

A particularly interesting strategy used in the design of metal-free DSSC dyes is to make push-pull molecules of the form D- $\pi$ -A where D is an electron donor,  $\pi$  is a conjugated spacer which serves as a molecular wire for conducting electrons to A, the electron acceptor. The push-pull structure reduces the risks of donor-acceptor electron recombination by promoting charge transfer and also accelerates the regeneration of the dye by the electrolyte. The push-pull strategy has been discussed for zinc porphyrins in Ref. [114] while Ref. [115] which studies the best spacers and the best length of spacers for *p*-type DSSCs. Other articles concerning the push-pull strategy in designing metal-free DSSC dyes include, but are not limited to, Refs. [116, 117, 118, 119, 120, 121, 122, 123, 124, 125, 126, 127, 128, 129, 130, 131, 132, 133, 134].

Yet another strategy for making metal-free DSSC dyes is seen in theoretical attempts to create organic dyes which will promote singlet fission (SF) [136]. In SF, an energetic photon is absorbed creating a singlet state which can subsequently split into two independent singlet or triplet excitations. These excitations can each interact with the  $\text{TiO}_2$  substrate to produce two electrons. PCE increases because for each photon absorbed two electrons are produced.

We now we wish to provide a simple example of how computational chemistry may be used in analyzing a series of candidate metal-free DSSC dyes [137]. To this end, we consider the three “push-pull” molecules based upon 2,2'-(1,4-phenylene)bis(quinazolin-4(3H)-imine) shown in Fig. 10. Each of these molecules consists of an electron acceptor A containing a carboxylic acid group that

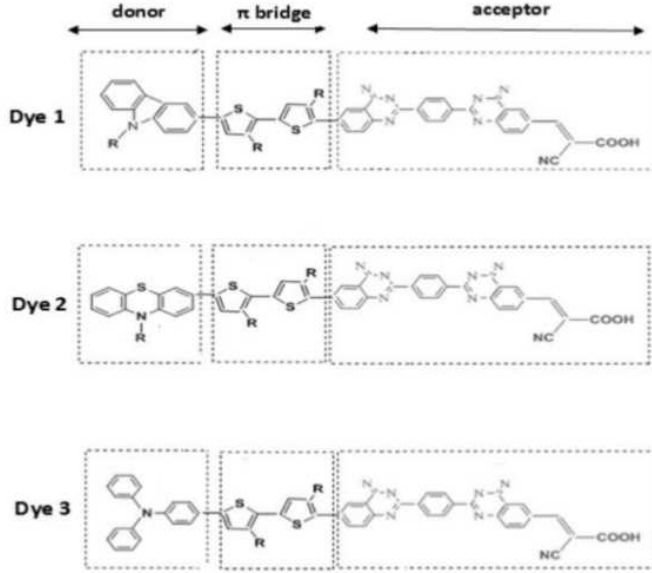


Figure 10: Chemical structures of the three push-pull dyes studied here, where R stands for the methyl group ( $\text{CH}_3$ ). The three dyes have the same  $\pi$ -spacer and acceptor unit, but differ by the donor unit: methylcarbazole for dye **1**, 10-phenothiazine for dye **2**, and triarylamine for dye **3**.

Dye	<b>1</b>	<b>2</b>	<b>3</b>
$E^{\text{dye}}$	-5.472 eV	-5.454 eV	-5.261 eV
$E^{\text{dye}^*}$	-2.692 eV	-2.704 eV	-2.611 eV
$\Delta G_{\text{inject}}$	1.308 eV	1.296 eV	1.389 eV

Table 2: Summary of some relevant energies for dyes **1**, **2**, and **3**.

can bind to  $\text{TiO}_2$  nanoparticles, a donor group D, and a  $\pi$ -bridge spacer group that also serves as a “molecular wire” for transferring electrons from D to A. Only D varies in this series of molecules while the  $\pi$ -bridge and A is held constant. We anticipate that a photon will create a charge separation creating a hole on D and an electron on A. This is consistent with the picture shown in Fig. 11(a). We are interested in factors that increase the PCE. From Eq. (3), this includes  $V_{oc}$  (also referred to as  $\Delta G_{\text{inject}}$  in this field) which is related to the difference between  $\epsilon_{\text{HOMO}}^A = -4.0$  eV for  $\text{TiO}_2$  [138] and  $\epsilon_{\text{LUMO}}^D$  for the dyes and may be thought of as the driving force for charge separation.

The geometries were first optimized at the B3LYP/6-31G(d) level in vacuum. The HOMO and LUMO energies were then obtained at the same level of calculation. All three dyes have more negative HOMO energies than the  $\text{I}^-/\text{I}_3^-$  redox couple (-4.8 eV [139]), indicating that a  $\text{I}^-/\text{I}_3^-$  solution is expected to be appropriate for quick regeneration of the ground state of the dye after electron transfer to the substrate. The ground state oxidation potentials of the three dyes were obtained in the approximation,  $E^{\text{dye}} = \epsilon_{\text{HOMO}}^{\text{dye}}$ . (Results are collected in Table 2.) Spectra were calculated at the TD-CAM-B3LYP/6-31G(d) level and the excitation energy  $\Delta E$  corresponding to the lowest energy absorption peak and corresponding oscillator strength  $f$  were obtained. The oxidation potential of the excited dye was calculated as  $E^{\text{dye}^*} = \epsilon_{\text{HOMO}}^{\text{dye}} + \Delta E$ . The resultant  $E^{\text{dye}^*}$  is from 0.27 eV to 0.38 eV higher in energy than the  $\epsilon_{\text{LUMO}}^{\text{dye}}$  calculated at the B3LYP/6-31G(d) level.

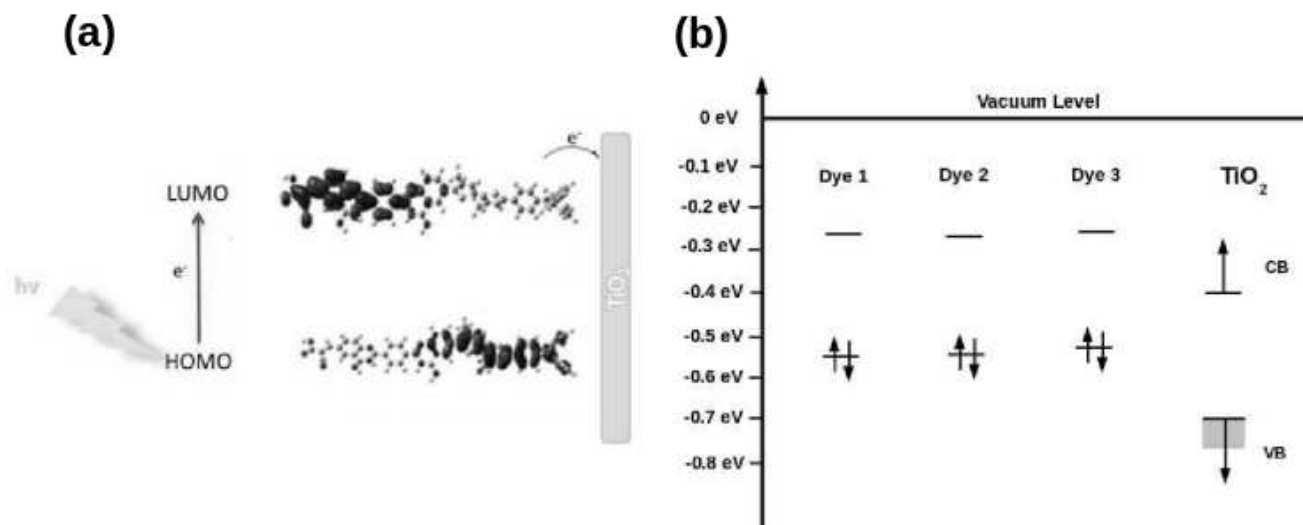


Figure 11: (a) Calculated DFT HOMO and LUMO densities for dye **3** illustrating the HOMO  $\rightarrow$  LUMO charge transfer that is expected to occur during the passage of an electron from the ground to the lowest excited singlet state. (b) Comparison of  $E^{\text{dye}}$  and  $E^{\text{dye}^*}$  for the three dyes with the  $\text{TiO}_2$  valence band (VB) and conduction band (CB) level.

Typically the charge-separation efficiency  $\Phi_{\text{inject}}$  within the active layer increases as  $\Delta G_{\text{inject}}$  increases. Figure 11(b) part of the story: An electron initially in the HOMO of the dye is excited to the LUMO of the dye. The calculated value of LHE given in Table 2 shows that this is an efficient charge-transfer process with values of LHE close to unity. As the LUMO of the dye is higher than the CB of the  $\text{TiO}_2$ , the electron jumps to the CB. The difference between the CB energy and the  $E^{\text{dye}^*}$  is related to the charge-separation momentum which will drive the electron into the  $\text{TiO}_2$ . As seen in Table 2,  $\Delta G_{\text{inject}}$  is highest for dye **3** and lowest for dye **2**, though the differences are not dramatic.

### 4.3 Metal-Free Organic Light-Emitting Diodes

In Sec. 3.3, we considered phosphorescent OLEDs that exploit the heavy-metal effect by incorporating iridium(III) complexes in their active layer. There is also some work on using Earth-abundant transition metals such as copper to make OLEDs [17]. However we wish to ask the question of how metals might be removed from the active layer and still have an efficient OLED? We will follow the conventional practice of calling this a metal-free (MF) OLED, though metals are always still present in the electrodes. Here, as in the other areas treated in this chapter, a heavy synergy between experiment and computational chemistry is strongly felt in this area as computational modeling is important for clarifying luminescence mechanisms and for providing ideas for improved luminescent molecules.

Several strategies are possible for making MF-OLEDs, but only a few will be mentioned here. Thus MF-OLEDs may be based upon either phosphorescence or upon fluorescence. Even in the MF case, OLEDs may take advantage of the heavy-atom effect by incorporating non-metal heavy atoms, such as bromine. This is the case of a MF-OLED reported by Lee, Han, and Lee [140]. This study is especially notable because the experimental work is complemented by TD-DFT calculations

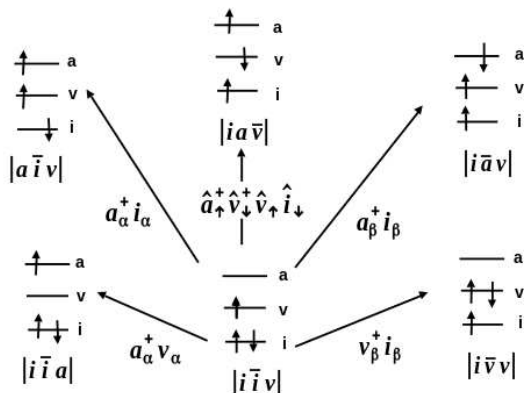


Figure 12: Three-hole three-electron model (TOTEM). See text for additional explanation.

characterizing the excited states and by molecular dynamics simulations to study structure and rigidity. It is also possible to make a phosphorescent MF-OLED without any heavy atom. This is possible because SOC is present, even though weaker than in the heavy-atom case, provided non-radiative pathways can be blocked [141]. A drawback of this latter strategy is that exploiting the long-lived phosphorescent state is not compatible with the high-driving intensities needed for intense lighting [141].

A better strategy for making MF-OLEDs is to base them on fluorescence rather than phosphorescence. There are at least two ways to do this. Molecules with a small enough  $S_1$ - $T_1$  gap can show thermally-activated delayed fluorescence (TADF). This simply means that the meeting of electrons and holes in the active layer produces both singlets and triplets but that the Boltzmann factor for thermal population of the singlet state from the triplet state is large enough that the triplet population drains away into the more rapidly luminescing singlet state. This is the strategy for the Earth-abundant copper complex-based OLED mentioned above [17] but has also been used in MF-OLEDs [142, 143]. A detailed theoretical mechanism for TADF in conjugated polymers is reported in Ref. [144].

Yet another strategy for making MF-OLEDs, and one that we choose to focus on here, is to make use of stable organic free radicals. Although the existence of stable organic free radicals does not seem to be widely known in the chemistry community outside of specialists in this area, stable organic free radicals have been studied since the 1900 landmark paper of Gomberg on the triphenylmethyl radical [145]. Since then many other stable organic free radicals have been discovered (Refs. [146, 147] provide useful reviews of different classes of stable organic free radicals). Recently stable organic radicals have been suggested as a way to make MF-OLEDs [148, 149, 150, 151, 152, 153].

In order to understand how this works, let us consider the TOTEM again, but this time, it is the three-electron three-level model shown in Fig. 12. This figure is to be understood as having been constructed using the spin-restricted open-shell Hartree-Fock (ROHF) method [154] [whose DFT equivalent is the spin-restricted open-shell Kohn-Sham (ROKS) method [155]], which basically may be understood in this case as using an orbital hamiltonian averaged over  $\alpha$  and  $\beta$  spins.

We are now free to study the excitation energies of such a system. The two lowest excited states are expected to arise from the  $i \rightarrow v$  and  $v \rightarrow a$  excitations, with the later expected to be of lower energy than the former if the general principle is respected that higher-lying orbitals have less orbital-energy separation than do lower-lying orbitals. This leads to two types of doublets, each arising from one of the two configurations,  $D_1 = {}^2(v, a)$  and  $D_2 = {}^2(i, v)$ . A detailed analysis (not shown here

lack of space) leads to the conclusion that the  $D_1$  excitation energy may be negative if the orbital energy difference is less than the corresponding coulomb repulsion integral,  $\epsilon_a - \epsilon_v < [aa|vv]$ . Thus the HOMO of the GS may be higher than the LUMO of the GS or, to use the language of solid-state physics, we may have a “hole below the Fermi energy.”

In principle, free radical MF-OLEDs could avoid the triplet/singlet spin-statistics problem because only doublet states are available at low excitation energies. Fluorescence would then occur from these to the ground state. Of course these ideas must be confirmed by experiment as other scenarios might be possible. For example, injection of a hole into the active layer before injection of an electron could conceivably lead to the formation of singlet and triplet intermediates. Fortunately a detailed experimental and theoretical study shows that this is not the case for at least one organic free radical MF-OLED [152]. We also note that the predicted possibility of a hole below the Fermi level has also been found [153].

## 5 Conclusion

This chapter has focused on some of the greenest areas of the energy sciences, namely the use of abundant solar energy and energy-efficient lighting and displays through light-emitting diodes. We have focused specifically on dye-sensitized solar cells and upon organic light-emitting diodes. Even this deliberately-chosen narrow scope has still left us with a very large area to review. Nevertheless we have made an effort to explain the basics of how devices work, how their efficiency is measured in practice, the key underlying photoprocesses. We have also taken pains to illustrate how computational chemistry is used hand-in-hand with experimental work to make better DSSCs and OLEDs by first considering conventional DSSCs and OLEDs based upon the heavy-metal effect, then by considering the replacement of rare metals with Earth-abundant metals, and finally by examining strategies for making metal-free DSSC dyes and OLED active layers. As might be expected from such an ambitious plan, we are deeply aware of what has not been treated and of what has only been treated shallowly. Nevertheless we hope and trust that this modest chapter will be helpful in showing how computational chemistry is actively helping to make the energy sciences more efficient, more sustainable, and more environmentally-friendly.

## Acknowledgement

DM and MEC gratefully acknowledge helpful funding from the French Embassy in Kenya and from the African School on Electronic Structure Methods and Applications (ASESMA). MT and KA gratefully acknowledge funding from the Government of Tunisia. Too many people have helped us over the years towards a better understanding of the topic of this chapter to be able to name them all here, but particular thanks go to the following for helpful discussions: Katja Heinze, Damien Jouvenot, Max Latévi Lawson Daku, Frédérique Loiseau, Cleophas Muhavini Wawire, and Xiuwen Zhou. The authors are grateful for computational resources provided by the *Plateau du Centre d'Expérimentation et de Calcul Intensif en Chimie (PCECIC)* of the *Institut de Chimie Moléculaire de Grenoble (ICMG)* at the *Université Grenoble Alpes (UGA)* where some of the calculations reported here were carried out.

## **Author Contributions**

MEC wrote sections 1 and 5 and subsections 4.1 and 4.3. DM wrote section 3.4 and subsections 3.1, 3.2, and 3.3. TM and KA wrote subsection 4.2. MEC coordinated the writing and was responsible for editing.

## References

- [1] G. B. Haxel, J. B. Hedrick, and G. J. Orris, [Rare earth elements—critical resources for high technology](#), United States Geological Survey Fact Sheet 087-02, 2002.
- [2] J. Michl and V. Bonačić-Koutecký, *Electronic Aspects of Organic Photochemistry*, John Wiley & Sons, Inc., New York, New York, 1990.
- [3] N. J. Turro, *Modern Molecular Photochemistry*, University Science Books, Mill Valley, Calif., 1991.
- [4] M. Klessinger and J. Michl, *Excited States and Photochemistry of Organic Molecules*, VCH Publishers, New York, New York, 1995.
- [5] N. J. Turro, V. Ramamurthy, and J. C. Scaiano, *Modern Molecular Photochemistry of Organic Molecules*, University Science Books, Sausalito, Calif., 2010.
- [6] M. Grätzel, [Recent advances in sensitized mesoscopic solar cells](#), *Acc. Chem. Res.* **42**, 1788 (2009).
- [7] W. Shockley and H. J. Queisser, [Detailed balance limit of efficiency of p-n junction solar cells](#), *J. Appl. Phys.* **32**, 510 (1961).
- [8] S. M. Sze and K. K. Ng, *Physics of Semiconductor Devices*, Wiley India, New Delhi, third edition, 2007.
- [9] S. C. Jain, W. Willander, and V. Kumar, *Conducting Organic Materials and Devices*, volume 81 of *Semiconductors and Semimetals*, Academic Press, New York, 2007.
- [10] N. C. Giebink, G. P. Viederrecht, M. R. Wasielewski, and S. R. Forrest, [Ideal diode equation for organic heterojunctions. I. Derivation and application](#), *Phys. Rev. B* **82**, 155305 (2010).
- [11] V. D. Mihailetschi, P. W. M. Blom, J. C. Hummelen, and M. T. Rispens, [Cathode dependence of the open-circuit voltage of polymer:fullerene bulk heterojunction solar cells](#), *J. Appl. Phys.* **94**, 6849 (2003).
- [12] A. A. M. H. M. Darghouth et al., [Assessment of density-functional tight-binding ionization potentials and electron affinities of molecules of interest for organic solar cells against first-principles \*gw\* calculations](#), *Computation* **3**, 616 (2015).
- [13] A. Mihi, F. J. López-Alcaraz, and H. Míguez, [Full spectrum enhancement of the light harvesting efficiency of dye sensitized solar cells by including colloidal photonic crystal multilayers](#), *Appl. Phys. Lett.* **88**, 193110 (2006).
- [14] J. Zhang et al., [Density functional theory characterization and design of high-performance diarylamine-fluorene dyes with different  \$\pi\$  spacers for dye-sensitized solar cells](#), *J. Mater. Chem.* **22**, 568 (2012).
- [15] M. C. Scharber et al., [Design rules for donors in bulk-heterojunction solar cells—Towards 10% energy-conversion efficiency](#), *Adv. Mater.* **18**, 789 (2006).
- [16] M. C. Scharber, [On the efficiency limit of conjugated polymer:fullerene-based bulk heterojunction solar cells](#), *Adv. Mater.* **28**, 1994 (2016).

- [17] H. Yersin, A. F. Rausch, R. Czerwieniec, T. Hofbeck, and T. Fischer, [The triplet state of organo-transition metal compounds. Triplet harvesting and singlet harvesting for efficient OLEDs](#), *Coord. Chem. Rev.* **255**, 2622 (2011).
- [18] J.-P. Sauvage et al., [Ruthenium\(II\) and osmium\(II\) bis\(terpyridine\) complexes in covalently-linked multicomponent systems: Synthesis, electrochemical behavior, absorption spectra, and photochemical and photophysical properties](#), *Chem. Rev.* **94**, 993 (1994).
- [19] A. Aviram and M. A. Ratner, [Molecular rectifiers](#), *Chem. Phys. Lett.* **29**, 277 (1974).
- [20] B. N. Figgis and M. A. Hitchman, *Ligand field theory and its applications*, Wiley-VCH, Weinheim, Germany, 2000.
- [21] D. Magero, M. E. Casida, G. Amolo, N. Makau, and L. Kituyi, [Partial density of states ligand field theory \(PDOS-LFT\): Recovering a LFT-like picture and application to photoproperties of ruthenium\(II\) polypyridine complexes](#), *J. Photochem. Photobiol. A* **348**, 305 (2017).
- [22] P. S. Wagenknecht and P. C. Ford, [Metal centered ligand field excited states: Their roles in the design and performance of transition metal based photochemical molecular devices](#), *Coord. Chem. Rev.* **255**, 591 (2011).
- [23] M. Ameloot, M. Vandeven, A. Ulises, and B. Valeur, [Time-resolved fluorescence anisotropy\(a\) b. valeur. molecular fluorescence. principles and applications, wileyVCH, weinheim \(2002\) \(b\) b. valeur, m. n. berberan- santos. molecular fluorescence. principles and applications, 2nd ed., wiley-VCH, weinheim \(2012\). j. r. lakowicz. principles of fluorescence spectroscopy, 3rd ed., springer, new york \(2006\).](#), 2016.
- [24] C. Wawire, *Theoretical Investigation of Ruthenium Photocatalysts*, Theses, Université de Grenoble, 2012.
- [25] X. Ma and H. Tian, [Photochemistry and photophysics. concepts, research, applications. by vincenzo balzani, paola ceroni and alberto juris.](#), *Angewandte Chemie International Edition* **53**, 8817 (2014).
- [26] C. M. Wawire et al., [Density-functional study of luminescence in polypyridine ruthenium complexes](#), *J. Photochem. and Photobiol. A* **276**, 8 (2014).
- [27] R. Hoffmann, *Solids and Surfaces: A Chemist's View of Bonding in Extended Structures*, VCH Publishers, New York, 1988.
- [28] B. O'Regan and M. Grätzel, [A low-cost, high-efficiency solar cell based on dye-sensitized colloidal TiO<sub>2</sub> films](#), *Nature* **353**, 737 (1991).
- [29] [Michael graetzel \(switzerland\) 2017](#), <https://globalenergyprize.org/en/laureates/2017/michael-graetz> Accessed: 2019-08-26.
- [30] M. Grätzel, [Dye-sensitized solar cells](#), *J. Photochem. Photobiol. C: Photochem. Rev.* **4**, 145 (2003).
- [31] D. Filippo, F. Simona, and G. Ralph, [Simulating dye-sensitized tio<sub>2</sub> heterointerfaces in explicit solvent: Absorption spectra, energy levels, and dye desorption](#), *The Journal of Physical Chemistry Letters* **2**, 813 (2011).

- [32] L. Rahul and S. M. Parasharam, *Fabrication of TiO<sub>2</sub> based dye-sensitized solar cell with natural dyes*, PhD thesis, Discipline of Physics, IIT Indore, 2019.
- [33] G. Smestad, [Testing of dye sensitized TiO<sub>2</sub> solar cells II: Theoretical voltage output and photoluminescence efficiencies](#), Sol. Energy Mater. Sol. Cells **32**, 273 (1994).
- [34] G. Smestad, C. Bignozzi, and R. Argazzi, [Testing of dye sensitized TiO<sub>2</sub> solar cells I: Experimental photocurrent output and conversion efficiencies](#), Sol. Energy Mater. Sol. Cells **32**, 259 (1994).
- [35] A. Kay and M. Grätzel, [Low cost photovoltaic modules based on dye sensitized nanocrystalline titanium dioxide and carbon powder](#), Solar Energy Mater. Solar Cells **44**, 99 (1996).
- [36] S. Y. Dai et al., [Dye-sensitized solar cells, from cell to module](#), Sol. Energy Mater. Sol. Cells **84**, 125 (2004).
- [37] J. Halme, M. Toivola, A. Tolvanen, and P. Lund, [Charge transfer resistance of spray deposited and compressed counter electrodes for dye-sensitized nanoparticle solar cells on plastic substrates](#), Sol. Energy Mater. Sol. Cells **90**, 872 (2006).
- [38] F. T. Kong, S. Y. Dai, and K. T. Wang, [New amphiphilic polypyridyl ruthenium\(II\) sensitizer and its application in dye-sensitized solar cells](#), Chin. J. Chem. **25**, 168 (2007).
- [39] J. Xia et al., [Influence of doped anions on poly\(3,4-ethylenedioxythiophene\) as hole conductors for iodine-free solid-state dye-sensitized solar cells](#), J. Am. Chem. Soc. **130**, 1258 (2008).
- [40] Y. Ooyama and Y. Harima, [Molecular designs and syntheses of organic dyes for dye-sensitized solar cells](#), Eur. J. Org. Chem. **18**, 2903 (2009).
- [41] J. Preat, [Photoinduced energy-transfer and electron-transfer processes in dye-sensitized solar cells: TDDFT insights for triphenylamine dyes](#), J. Phys. Chem. C **114**, 16716 (2010).
- [42] C. Wang et al., [Performance improvement of dye-sensitizing solar cell by semi-rigid triarylamine-based donors](#), Dyes Pigments **94**, 40 (2012).
- [43] A. Hagfeldt, G. Boschloo, L. C. Sun, L. Kloo, and H. Pettersson, [Dye-sensitized solar cells](#), Chem. Rev. **110**, 6595 (2010).
- [44] Z. Ning and H. Tian, [Triarylamine: a promising core unit for efficient photovoltaic materials](#), Chem. Commun. (Cambridge) **37**, 5483 (2009).
- [45] A. Mishra, M. K. R. Fischer, and P. Bauerle, [Metal-free organic dyes for dye-sensitized solar cells: from structure-property relationships to design rules](#), Chem. Int. Ed. **48**, 2474 (2009).
- [46] J. Preat, D. Jacquemin, and E. A. Perpete, [Design of new triphenylamine-sensitized solar cells: a theoretical approach](#), Sci. Technol. **44**, 5666 (2010).
- [47] M. Ye et al., [Recent advances in dye-sensitized solar cells: from photoanodes, sensitizers and electrolytes to counter electrodes](#), Materials Today **18**, 155 (2015).
- [48] M. A. Green et al., [Solar cell efficiency tables \(version 52\)](#), Progress in Photovoltaics: Research and Applications **26**, 427 (2018).

- [49] M. K. Nazeeruddin et al., [Engineering of efficient panchromatic sensitizers for nanocrystalline TiO<sub>2</sub>-based solar cells](#), *J. Am. Chem. Soc.* **123**, 1613 (2001).
- [50] Z. Wang, T. Yamaguchi, H. Sugihara, and H. Arakawa, [Significant efficiency improvement of the black dye-sensitized solar cell through protonation of TiO<sub>2</sub> films](#), *Langmuir* **21**, 4272 (2005).
- [51] K. Sodeyama et al., [Protonated carboxyl anchor for stable adsorption of Ru N749 dye \(black dye\) on a TiO<sub>2</sub> anatase \(101\) surface](#), *J. Phys. Chem. Lett.* **3**, 472 (2012).
- [52] Y. Tateyama et al., [Acetonitrile solution effect on Ru N749 dye adsorption and excitation at TiO<sub>2</sub> anatase interface](#), *J. Phys. Chem. C* **118**, 16863 (2014).
- [53] C. Adachi, [Third-generation organic electroluminescence materials](#), *Japanese Journal of Applied Physics* **53**, 060101 (2014).
- [54] M. A. Baldo, S. Lamansky, P. E. Burrows, M. E. Thompson, and S. R. Forrest, [Very high-efficiency green organic light emitting devices based on electrophosphorescence](#), *J. Appl. Phys.* **75**, 5048 (1999).
- [55] A. F. Rausch, H. Homeier, P. I. Djurovich, M. E. Thompson, and H. Yersin, [Spin-orbit coupling routes and OLED performance: studies of blue-light emitting ir\(III\) and pt\(II\) complexes](#), in *Organic Light Emitting Materials and Devices XI*, edited by Z. H. Kafafi and F. So, SPIE, 2007.
- [56] J. A. G. Williams, [Photochemistry and photophysics of coordination compounds: Platinum](#), in *Photochemistry and Photophysics of Coordination Compounds II*, pages 205–268, Springer Berlin Heidelberg, 2007.
- [57] S. Lo et al., [Blue phosphorescence from iridium\(III\) complexes at room temperature](#), *Chem. Mater.* **18**, 5119 (2006).
- [58] U. Giovanella, M. Pasini, and C. Botta, [Organic light-emitting diodes \(OLEDs\): Working principles and device technology](#), in *Lecture Notes in Chemistry*, pages 145–196, Springer International Publishing, 2016.
- [59] N. Su and Y. Zheng, [Four-membered red iridium\(III\) complexes with Ir–S–P–S structures: rapid room-temperature synthesis and application in OLEDs](#), *Dalton Transactions* **48**, 7583 (2019).
- [60] Y. Chi, T. Chang, P. Ganesan, and P. Rajakannu, [Emissive bis-tridentate Ir\(III\) metal complexes: Tactics, photophysics and applications](#), *Coord. Chem. Rev.* **346**, 91 (2017).
- [61] S. Yun, J. Jeon, S. Jin, S. K. Kang, and Y. Kim, [Synthesis, structure, and OLEDs application of cyclometalated iridium\(III\) complexes utilizing substituted 2-phenylpyridine](#), *Bull. Korean Chem. Soc.* **38**, 788 (2017).
- [62] C. Adachi, M. A. Baldo, and S. R. Forrest, [High-efficiency organic electrophosphorescent devices with tris\(2-phenylpyridine\)iridium doped into electron-transporting materials](#), *Appl. Phys. Lett.* **77**, 904 (2000).
- [63] S. Lo et al., [High-triplet-energy dendrons: Enhancing the luminescence of deep blue phosphorescent iridium\(III\) complexes](#), *J. Am. Chem. Soc.* **131**, 16681 (2009).
- [64] T. Sajoto et al., [Temperature dependence of blue phosphorescent cyclometalated Ir\(III\) complexes](#), *J. Am. Chem. Soc.* **131**, 9813 (2009).

- [65] A. R. G. Smith et al., [Effects of fluorination on iridium\(III\) complex phosphorescence: Magnetic circular dichroism and relativistic time-dependent density functional theory](#), *Inorg. Chem.* **51**, 2821 (2012).
- [66] J. Lee et al., [Deep blue phosphorescent organic light-emitting diodes with very high brightness and efficiency](#), *Nat. Mater.* **15**, 92 (2016).
- [67] Q. Peng et al., [Understanding the efficiency drooping of the deep blue organometallic phosphors: a computational study of radiative and non-radiative decay rates for triplets](#), *J. Mater. Chem. C* **4**, 6829 (2016).
- [68] X. Zhou, P. L. Burn, and B. J. Powell, [Bond fission and non-radiative decay in iridium\(III\) complexes](#), *Inorg. Chem.* **55**, 5266 (2016).
- [69] X. Zhou, P. L. Burn, and B. J. Powell, [Effect of \*n\*-propyl substituents on the emission properties of blue phosphorescent iridium\(III\) complexes](#), *J. Chem. Phys.* **146**, 174305 (2017).
- [70] X. Zhou and B. J. Powell, [Nonradiative decay and stability of \*n\*-heterocyclic carbene iridium\(III\) complexes](#), *Inorg. Chem.* **57**, 8881 (2018).
- [71] L. Flamigni, A. Barbieri, C. Sabatini, B. Ventura, and F. Barigelletti, [Photochemistry and photophysics of coordination compounds: Iridium](#), in *Photochemistry and Photophysics of Coordination Compounds II*, edited by V. Balzani and S. Campagna, page 143, Springer Berlin Heidelberg, 2007.
- [72] A. Juris et al., [Ru\(II\) polypyridine complexes: Photophysics, photochemistry, electrochemistry, and chemiluminescence](#), *Coord. Chem. Rev.* **84**, 85 (1988).
- [73] L. G. Vanquickenborne and A. Ceulemans, [Ligand-field models and the photochemistry of coordination compounds](#), *Coord. Chem. Rev.* **48**, 157 (1982).
- [74] K. Müller, [Reaction paths on multidimensional energy hypersurfaces](#), *Angew. Chem. Int. Ed. Engl.* **19**, 1 (1980).
- [75] I. M. Dixon, J. Heully, F. Alary, and P. I. P. Elliott, [Theoretical illumination of highly original photoreactive <sup>3</sup>MC states and the mechanism of the photochemistry of Ru\(II\) tris\(bidentate\) complexes](#), *Phys. Chem. Chem. Phys.* **19**, 27765 (2017).
- [76] Q. Sun, B. Dereka, E. Vauthey, L. M. L. Daku, and A. Hauser, [Ultrafast transient IR spectroscopy and DFT calculations of ruthenium\(II\) polypyridyl complexes](#), *Chem. Sci.* **8**, 223 (2017).
- [77] A. Soupart, I. M. Dixon, F. Alary, and J. Heully, [DFT rationalization of the room-temperature luminescence properties of Ru\(bpy\)<sub>3</sub><sup>2+</sup> and Ru\(tpy\)<sub>3</sub><sup>2+</sup>: <sup>3</sup>MLCT-<sup>3</sup>MC minimum energy path from NEB calculations and emission spectra from VRES calculations](#), *Theor. Chem. Acc.* **137**, 37 (2018).
- [78] A. Fouqueau et al., [Comparison of density functionals for energy and structural differences between the high \[<sup>5</sup>T<sub>2g</sub>: \(t<sub>2g</sub>\)<sup>4</sup>\(e<sub>g</sub>\)<sup>2</sup>\] and Low \[<sup>1</sup>A<sub>1g</sub>: \(t<sub>2g</sub>\)<sup>6</sup>\(e<sub>g</sub>\)<sup>0</sup>\] Spin States of the Hexaquoferrous Cation, \[Fe\(H<sub>2</sub>O\)<sub>6</sub>\]<sup>2+</sup>](#), *J. Chem. Phys.* **120**, 9473 (2004).
- [79] C. Degli Esposti and L. Bizzocchi, [Absorption and emission spectroscopy of a lasing material: ruby](#), *J. Chem. Ed.* **84**, 1316 (2007).

- [80] S. Otto, M. Grabolle, C. Förster, C. Kreitner, and U. R. and K. Heinze, [\[Cr\(ddpd\)<sub>2</sub>\]<sup>3+</sup>: A molecular, water-soluble, high NIR-emissive ruby analogue](#).
- [81] J. M. R. Narayanam and C. R. J. Stephenson, [Visible light photoredox catalysis: applications in organic synthesis](#), Chem. Soc. Rev. **40**, 102 (2011).
- [82] D. M. Arias-Rotondo and J. K. McCusker, [The photophysics of photoredox catalysis: a roadmap for catalyst design](#), Chem. Soc. Rev. **45**, 5803 (2016).
- [83] K. A. King, P. J. Spellane, and R. J. Watts, [Excited-state properties of a triply ortho-metalated iridium\(III\) complex](#), J. Am. Chem. Soc. **107**, 1431 (1985).
- [84] S. Otto et al., [Photochromium: Sensitizer for visiblelightinduced oxidative CH bond functionalizationelectron or energy transfer?](#), ChemPhotoChem **1**, 344 (2017).
- [85] S. Otto, N. Scholz, T. Behnke, U. Resch-Genger, and K. Heinze, [Thermochromium: A contactless optical molecular thermometer](#), Chem. Eur. J. **23**, 12131 (2017).
- [86] S. Otto, J. P. Harris, K. Heinze, and C. Reber, [Molecular ruby under pressure](#), Angew. Chem. Int. Ed. **57**, 11069 (2018).
- [87] C. B. Larsen and O. S. Wenger, [Photoredox catalysis with metal complexes made from Earth-abundant elements](#), Chem. Eur. J. **24**, 2039 (2018).
- [88] O. Johnson, *Guide Delachaux des minéraux*, Delachaux et Niestlé, Paris, 2006, translated from Danish into French by J.-P. Poirot.
- [89] O. Johnsen, *Mineralernes Verden*, Gyldendalske Boghandel, Nordisk Forlag, Copenhagen, 2000.
- [90] T. H. Maiman, [Stimulated optical radiation in ruby](#), Nature **187**, 493 (1960).
- [91] C. H. Townes, *How the Laser Happened*, Oxford University Press, New York, 1999.
- [92] C. Förster et al., [Ddpd as expanded terpyridine: Dramatic effects of symmetry and electronic properties in first row transition metals](#), Inorganics **6**, 86 (2018).
- [93] C. Wang et al., [Deuterated molecular ruby with record luminescence quantum yield](#), Angew. Chem. Int. Ed. **57**, 1112 (2018).
- [94] A. Breivogel, C. Förster, and K. Heinze, [A heteroleptic bis\(tridentate\)ruthenium\(II\) polypyridine complex with improved photophysical properties and integrated functionalizability](#), Inorg. Chem. **49**, 7052 (2010).
- [95] L. Zeng et al., [The development of anticancer ruthenium\(II\) complexes: from single molecule compounds to nanomaterials](#), Chem. Soc. Rev. **46**, 5771 (2017).
- [96] C. G. Garcia, A. S. Polo, and N. Y. M. Iha, [Photoelectrochemical solar cell using extract of \*eugenia jambolana lam\* as a natural sensitizer](#), J. Anais da Academia Brasileira de Ciências **75**, 163 (2003).
- [97] N. J. Cherepy, G. P. Smestad, M. Grätzel, and J. Z. Zhang, [Ultrafast electron injection: Implications for a photoelectrochemical cell utilizing an anthocyanin dye-sensitized TiO<sub>2</sub> nanocrystalline electrode](#), J. Phys. Chem. B **101**, 9342 (1997).

- [98] M. Johal, [Fabrication of a dye-sensitized solar cell](https://www.youtube.com/watch?v=8hertoGXWtE), <https://www.youtube.com/watch?v=8hertoGXWtE>, last accessed 19 July 2019.
- [99] M. R. Narayan, [Review: Dye sensitized solar cells based on natural photosensitizers](#), *Renew. Sust. Energ. Rev.* **16**, 208 (2012).
- [100] N. A. Ludin et al., [Review on the development of natural dye photosensitizer for dye-sensitized solar cells](#), *Renew. Sustain. Energy Rev* **31**, 386 (2014).
- [101] N. T. R. N. Kumera, A. Lim, S. M. Lim, M. I. Petra, and P. Ekanayake, [Recent progress and utilization of natural pigments in dye sensitized solar cells: A review](#), *Renew. Sust. Energ. Rev.* **78**, 301 (2017).
- [102] G. Richhariya, A. Kumar, P. Tekasakul, and P. Gupta, [Natural dyes for dye sensitized solar cell: A review](#), *Renew. Sust. Energ. Rev.* **69**, 705 (2017).
- [103] P. Luo et al., [From salmon pink to blue natural sensitizers for solar cells: \*Canna indica L.\*, \*salvia splendens\*, \*cowberry\* and \*solanum nigrum l.\*](#), *Spectrochim. Acta A: Molec. Biomolec. Spectro.* **74**, 936 (2009).
- [104] F. D. Angelis, S. Fantacci, and R. Gebauer, [Simulating dye-sensitized TiO<sub>2</sub> heterointerfaces in explicit solvent: Absorption spectra, energy levels, and dye desorption](#), *J. Phys. Chem. Lett.* **2**, 813 (2011).
- [105] D. H. Douma and R. Gebauer, [Optical properties of dye sensitized TiO<sub>2</sub> nanowires from time-dependent density functional theory](#), *Phys. Status Solidi RRL* **5**, 259 (2011).
- [106] R. Gebauer and F. D. Angelis, [A combined molecular dynamics and computational spectroscopy study of a dye-sensitized solar cell](#), *New J. Phys.* **13**, 085013 (2011).
- [107] D. H. Douma, B. M'Passi-Mabiala, and R. Gebauer, [Optical properties of an organic dye from time-dependent density functional theory with explicit solvent: The case of alizarin](#), *J. Chem. Phys.* **137**, 154314 (2012).
- [108] M. Lee, M. P. Balanay, and D. H. Kim, [Molecular design of distorted push-pull porphyrins for dye-sensitized solar cells](#), *Theor. Chem. Acc.* **131**, 6623 (2012).
- [109] C. Lee et al., [Recent progress in organic sensitizers for dye-sensitized solar cells](#), *RSC Adv.* **5**, 23810 (2015).
- [110] W. Zhang et al., [Rational design of high-efficiency organic dyes in dye-sensitized solar cells by multiscale simulations](#), *Phys. Chem. C* **12244**, 25219 (2018).
- [111] Y. Cui, Y. Tong, L. Han, J. Gao, and J. Feng, [Design and photoelectric properties of D-A- \$\pi\$ -A carbazole dyes with different  \$\pi\$ -spacers and acceptors for use in solar cells: a DFT and TD-DFT investigation](#), *J. Mol. Model.* **25**, 249 (2019).
- [112] W. Shao et al., [Molecular design and application of novel small molecule organic dyes featuring bis\(arylvinyl\)phenyl amino group for dye-sensitized solar cells](#), *Solar Energy* **189**, 450 (2019).
- [113] G. C. Santos, E. F. Oliveira, F. C. Lavarda, and L. C. Silva-Filho, [Designing new quinoline-based organic photosensitizers for dye-sensitized solar cells \(DSSC\): a theoretical investigation](#), *J. Molec. Modeling* **25**, 1 (2019).

- [114] J. Lu, S. Liu, and M. Wang, [Push-pull zinc porphorins as light-harvesters for efficient dye-sensitized solar cells](#), *Front. Chem.* **6**, 541 (2018).
- [115] A. Sen and A. Groß, [Does involving additional linker always increase the efficiency of an organic dye for \*p\*-type dye-sensitized solar cells?](#), *ACS Appl. Energy Mater.* **2**, 6341 (2019).
- [116] W. Liu et al., [Simple organic molecules bearing a 3,4-ethylenedioxythiophene linker for efficient dye-sensitized solar cells](#), *Chem. Commun.* **2008**, 5152 (2008).
- [117] M. Xu et al., [Energy-level and molecular engineering of organic D- \$\pi\$ -A sensitizers in dye-sensitized solar cells](#), *J. Phys. Chem. C* **112**, 19770 (2008).
- [118] R. Li et al., [Dye-sensitized solar cells based on organic sensitizers with different conjugated linkers: furan, bifuran, thiophene, bithiophene, selenophene, and biselenophene](#), *J. Phys. Chem. C* **113**, 17 (2009).
- [119] G. Zhang et al., [High efficiency and stable dye-sensitized solar cells with an organic chromophore featuring a binary  \$\pi\$ -conjugated spacer](#), *Chem. Commun.* **2019**, 5152 (2009).
- [120] G. Zhang et al., [Employ a bithienothiophene linker to construct an organic chromophore for efficient and stable dye-sensitized solar cells](#), *Energy Environ. Sci.* **2**, 92 (2009).
- [121] J. Chen et al., [Organic dyes containing a coplanar indacenodithiophene bridge for high-performance dye-sensitized solar cells](#), *J. Org. Chem.* **76**, 8977 (2011).
- [122] Z. Ji, G. Natu, Z. Huang, and Y. Wu, [Linker effect in organic donor-acceptor dyes for \*p\*-type NiO dye sensitized solar cells](#), *Energy Environ. Sci.* **4**, 2818 (2011).
- [123] S. Namuangruk et al., [D-D- \$\pi\$ -A-type organic dyes for dye-sensitized solar cells with a potential for direct electron injection and a high extinction coefficient: Synthesis, characterization, and theoretical investigation](#), *J. Phys. Chem. C* **116**, 25653 (2012).
- [124] S. Mathew et al., [Dye-sensitized solar cells with 13% efficiency achieved through the molecular engineering of porphyrin sensitizers](#), *Nat. Chem.* **6**, 242 (2014).
- [125] H. Xia, J. Wang, F. Bai, and H. Zhang, [Theoretical studies of electronic and optical properties of the triphenylamine-based organic dyes with diketopyrrolopyrrole chromophore](#), *Dyes Pigm.* **113**, 87 (2015).
- [126] F. Zhang, P. Yu, W. Shen, M. Li, and R. He, [Effect of “push-pull” sensitizers with modified conjugation bridges on the performance of \*p\*-type dye-sensitized solar cells](#), *RSC Adv.* **5**, 64378 (2015).
- [127] A. K. Biswas, A. Das, and B. Ganguly, [Can fused-pyrrole rings act as better  \$\pi\$ -spacer units than fused-thiophene in dye-sensitized solar cells? a computational study](#), *New J. Chem.* **40**, 9304 (2016).
- [128] J. Ni, Y. Yen, and J. T. Lin, [Organic sensitizers with a rigid dithionobenzotriazole-based spacer for high-performance dye-sensitized solar cells](#), *J. Mater. Chem. A* **4**, 6553 (2016).
- [129] P. Li, Z. Wang, C. Song, and H. Zhang, [Rigid fused  \$\pi\$ -spacers in D- \$\pi\$ -A type molecules for dye-sensitized solar cells: a computational investigation](#), *J. Mater. Chem. C* **5**, 11454 (2017).

- [130] J. Ji, H. Zhou, and H. K. Kim, [Rational design criteria for D \$\pi\$ A structured organic and porphyrin sensitizers for highly efficient dye-sensitized solar cells](#), *J. Mater. Chem. A* **6**, 14518 (2018).
- [131] P. Heng et al., [Rational design of D- \$\pi\$ -A organic dyes to prevent "trade off" effect in dye-sensitized solar cells](#), *Spectrochim. Acta A* **221**, 117167 (2019).
- [132] H. Liu, B. Li, B. Xue, and E. Liu, [Theoretical design of D- \$\pi\$ -A-A sensitizers with narrow band gap and broad spectral response based on boron dipyrromethene for dye-sensitized solar cells](#), *J. Phys. Chem. C* **123**, 26047 (2019).
- [133] A. Sen and A. Groß, [Promising sensitizers for dye sensitized solar cells: A comparison of Ru\(II\) with other earth's scarce and abundant metal polypyridine complexes](#), *Int. J. Quant. Chem.* **119**, e25963 (2019).
- [134] H. Zhou et al., [Molecular design and synthesis of D \$\pi\$ A structured porphyrin dyes with various acceptor units for dye-sensitized solar cells](#), *J. Mater. Chem. C* **7**, 2843 (2019).
- [135] T. Bessho, S. M. Zakeeruddin, C.-Y. Yeh, E. W. Diau, and M. Grätzel, [Highly efficient mesoscopic dyesensitized solar cells based on donor-acceptorsubstituted porphyrins](#), *Angew. Chem. Int. Ed. Engl.* **49**, 6646 (2010).
- [136] D. Padula, O. H. Omar, T. Nemataram, and A. Troisi, [Singlet fission molecules among known compounds: finding a few needles in a haystack](#), *Energy Env. Sci.*, 2019.
- [137] T. Mestiri, *Prédiction de nouveaux copolymères pour l'électronique organique*, PhD thesis, Université de Monastir, 2019.
- [138] J. B. Asbury, Y. Q. Wang, E. Hao, H. Ghosh, and T. Lian, [Evidences of hot excited state electron injection from sensitizer molecules to TiO<sub>2</sub> nanocrystalline thin films](#), *Res. Chem. Intermed.* **27**, 393 (2001).
- [139] A. Hagfeldt and M. Grätzel, [Light-induced redox reactions in nanocrystalline systems](#), *Chem. Rev.* **95**, 49 (1995).
- [140] D. R. Lee, S. H. Han, and J. Y. Lee, [Metal-free and purely organic phosphorescent light-emitting diodes using phosphorescence harvesting hosts and organic phosphorescent emitters](#), *J. Mater. Chem. C* **7**, 11500 (2019).
- [141] D. Chaudhuri et al., [Metal-free OLED triplet emitters by side-stepping kasha's rule](#), *Angew. Chem. Int. Ed.* **52**, 13449 (2013).
- [142] H. Uoyama, K. Goushi, K. Shizu, H. Nomura, and C. Adachi, [Highly efficient organic light-emitting diodes from delayed fluorescence](#), *Nature* **492**, 234 (2012).
- [143] Y. Kim, C. Wolf, H. Cho, S. Jeong, and T. Lee, [Highly efficient, simplified, solution-processed thermally activated delayed-fluorescence organic light-emitting diodes](#), *Adv. Mater.* **28**, 734 (2016).
- [144] D. Beljonne, Z. Shuai, G. Pourtois, and J. L. Brédas, [Spin-orbit coupling and intersystem crossing in conjugated polymers: a configuration interaction description](#), *J. Phys. Chem. A* **105**, 3899 (2001).
- [145] M. Gomberg, [An instance of trivalent carbon: triphenylmethyl](#), *J. Am. Chem. Soc.* **22**, 757 (1900).

- [146] E. M. Kosower, [Stable pyridinyl radicals](#), *Top. Curr. Chem.* **112**, 117 (1983).
- [147] R. G. Hicks, [What's new in stable radical chemistry?](#), *Org. Biomol. Chem.* **5**, 1321 (2017).
- [148] Y. Hattori, T. Kusamoto, and H. Nishihara, [Luminescence, stability, and proton response of an openshell \(3,5dichloro4pyridyl\)bis\(2,4,6trichlorophenyl\)methyl radical](#), *Angew. Chem. Int. Ed.* **53**, 11845 (2014).
- [149] Y. Hattori, T. Kusamoto, and H. Nishihara, [Enhanced luminescent properties of an open-shell \(3,5-dichloro-4-pyridyl\)bis\(2,4,6-trichlorophenyl\)methyl radical by coordination to gold](#), *Angew. Chem. Int. Ed.* **54**, 3731 (2015).
- [150] Q. Peng, A. Obolda, M. Zhang, and F. Li, [Organic light-emitting diodes using a neutral  \$\pi\$  radical as emitter: The emission from a doublet](#), *Angew. Chem. Int. Ed.* **54**, 7091 (2015).
- [151] A. Obolda, Z. A. andd M. Zhang, and F. Li, [Up to 100% formation ratio of doublet exciton in deep-red organic light-emitting diodes based on neutral  \$\pi\$ -radical](#), *ACS Appl. Mater. Interfaces* **8**, 35472 (2016).
- [152] X. Ai et al., [Efficient radical-based light-emitting diodes with doublet emission](#), *Nature* **563**, 536 (2018).
- [153] H. Guo et al., [High stability and luminescence efficiency in donor-acceptor neutral radicals not following the Aufbau principle](#), <https://doi.org/10.1038/s41563-019-0433-1>, 2019.
- [154] C. C. J. Roothaan, [Self-consistent field theory for open shells of electronic systems](#), *Rev. Mod. Phys.* **32**, 179 (1960).
- [155] T. V. Russo, R. L. Martin, and P. J. Hay, [Density functional calculations on first-row transition metals](#), *J. Chem. Phys.* **101**, 7729 (1994).
- [156] H. Myneni and M. E. Casida, [On the calculation of  \$\Delta\langle\hat{S}^2\rangle\$  for electronic excitations in time-dependent density-functional theory](#), *Comput. Phys. Comm.* **213**, 72 (2017).